Article

Neuron

Dopamine Regulation of Amygdala Inhibitory Circuits for Expression of Learned Fear

Highlights

- LTD is induced in the LA-dorsal ITC synapses after weak fear conditioning
- LTD at the dorsal ITC depends upon D4R activity and the increased release of GABA
- Both ablation of D4R and reversal of LTD at the dorsal ITC lead to heightened fear
- LTD is impaired at the dorsal ITC of animals exhibiting PTSD-like behavior

Authors

Oh-Bin Kwon, Joo Han Lee, Hyun Jin Kim, ..., Craig H. Bailey, Eric R. Kandel, Joung-Hun Kim

Correspondence

joungkim@postech.ac.kr

In Brief

Kwon et al. identify activity-dependent synaptic plasticity at the dorsal ITC of the amygdala, which depends upon dopamine-mediated increases in inhibitory inputs. D4R-mediated LTD serves to demarcate the range of emotional stimuli that can be retained as long-term memory.

Kwon et al., 2015, Neuron *88*, 378–389
October 21, 2015
http://dx.doi.org/10.1016/j.neuron.2015.09.001

CellPress

CellPress

Neuron
Article

Dopamine Regulation of Amygdala Inhibitory Circuits for Expression of Learned Fear

Oh-Bin Kwon,[1,2,6] Joo Han Lee,[1,6] Hyun Jin Kim,[1] Seungho Lee,[1] Sanghyeon Lee,[1] Min-Jae Jeong,[1] Su-Jeong Kim,[1] Hee-Jung Jo,[1] Bumjin Ko,[1] Sunghoe Chang,[3] Sang Ki Park,[1] Yun-Beom Choi,[4] Craig H. Bailey,[4] Eric R. Kandel,[4,5] and Joung-Hun Kim[1,*]

[1]Department of Life Sciences, Pohang University of Science and Technology (POSTECH), Pohang, Gyungbuk 37673, Korea
[2]Daegu-Gyeongbuk Medical Innovation Foundation, New Drug Development Center, Daegu 41061, Korea
[3]Department of Physiology, College of Medicine, Seoul National University, Seoul 03080, Korea
[4]Department of Neuroscience, Kavli Institute of Brain Science, College of Physicians and Surgeons of Columbia University, New York State Psychiatric Institute, New York, NY 10032, USA
[5]Howard Hughes Medical Institute, New York, NY 10032, USA
[6]Co-first author
*Correspondence: joungkim@postech.ac.kr
http://dx.doi.org/10.1016/j.neuron.2015.09.001

SUMMARY

GABAergic signaling in the amygdala controls learned fear, and its dysfunction potentially contributes to posttraumatic stress disorder (PTSD). We find that sub-threshold fear conditioning leads to dopamine receptor D4-dependent long-term depression (LTD) of glutamatergic excitatory synapses by increasing inhibitory inputs onto neurons of the dorsal intercalated cell mass (ITC) in the amygdala. Pharmacological, genetic, and optogenetic manipulations of the amygdala regions centered on the dorsal ITC reveal that this LTD limits less salient experiences from forming persistent memories. In further support of the idea that LTD has preventive and discriminative roles, we find that LTD at the dorsal ITC is impaired in mice exhibiting PTSD-like behaviors. These findings reveal a novel role of inhibitory circuits in the amygdala, which serves to dampen and restrict the level of fear expression. This mechanism is interfered with by stimuli that give rise to PTSD and may also be recruited for fear-related psychiatric diseases.

INTRODUCTION

The amygdala is a brain region critical for acquisition and expression of conditioned fear whereby a neutral conditioned stimulus (CS) becomes associated with a noxious unconditioned stimulus (US) (Rogan et al., 1997). Among several nuclei that constitute the amygdala complex, it is the lateral nucleus (LA) that receives sensory inputs during fear conditioning, and after being associated in the LA, the signals are transmitted to the central nucleus (CeA) either directly or via the basal nucleus (Ehrlich et al., 2009; Palomares-Castillo et al., 2012; Pare and Duvarci, 2012; Lee et al., 2013). The intercalated cell masses (ITCs), which are situated between the amygdala nuclei encompassing the dorsal, ventral, and lateral clusters, appear to play a regulatory role in fear-related behavior by controlling the signal transfer between those amygdala nuclei. Thus, saponin-mediated lesions of ITCs or pharmacological inhibition of basolateral amygdala (BLA) inputs to ITCs interferes with extinction of fear memory (Likhtik et al., 2008; Jüngling et al., 2008). Although extinction of fear memory strengthens the excitatory inputs from the BLA to the ventral ITC (Amano et al., 2010), it remains unclear whether synaptic plasticity arising at the dorsal ITC can modulate fear acquisition and expression.

The dorsal ITC residing between the LA and CeA receives glutamatergic inputs from LA as well as from cortical regions, and it provides GABAergic inhibitory outputs to the lateral sector of the CeA and the ventral ITC (Ehrlich et al., 2009). By contrast, the ventral ITC receives its major inputs from the basal nucleus of the amygdala and sends projections to the medial sector of the CeA (Pare and Duvarci, 2012). The differences in connectivity of individual ITCs suggest that each ITC can play distinct roles in the regulation of fear behavior. Indeed, it has been proposed that the dorsal ITC regulates fear expression while the ventral ITC controls fear extinction (Busti et al., 2011; Duvarci and Pare, 2014). This raises the possibility that synaptic plasticity in the dorsal ITC could modify fear-related signaling from the LA to the CeA and the ensuing behavior and that deficits in the plastic capabilities of the dorsal ITC could potentially contribute to fear-related psychiatric diseases such as posttraumatic stress disorder (PTSD).

By modulating the activity of amygdala neurons, dopaminergic neurons can control the expression of fear memory (Fadok et al., 2009; de la Mora et al., 2010). Consistent with this notion, a subset of dopaminergic neurons is robustly activated on the presentation of aversive stimuli, and their firing rates positively correlate with the intensity or salience of the stimulus (Wang and Tsien, 2011). Dopamine (DA) gates synaptic plasticity in the amygdala and ultimately controls acquisition of fear memory by reducing feed-forward inhibition to LA projection neurons by means of DA-mediated increases in disynaptic inhibitory postsynaptic currents (IPSCs) in the local interneurons

(Rosenkranz and Grace, 2002; Bissière et al., 2003). As with the local interneurons within the BLA, the output of ITCs also can be regulated by DA (Marowsky et al., 2005). Although the dorsal ITC receives potent dopaminergic inputs (Fuxe et al., 2003), the DA-dependent long-term synaptic plasticity in the dorsal ITC circuit has not been explored.

We therefore assessed synaptic plasticity at the dorsal ITC using the stimulation protocol for spike-timing-dependent plasticity (STDP) (Shin et al., 2006). STDP stimulation induces long-term depression (LTD) in the LA-dorsal ITC pathway after weak fear conditioning, but not after strong fear conditioning. Induction of LTD at the dorsal ITC depends upon activation of dopamine receptor subtype 4 (D4R) and the concomitant enhancement in GABA release from neighboring ITC neurons. Importantly, selective blockade or depletion of D4R at the region of amygdala centered on the dorsal ITC or optogenetic manipulation that reverses the LTD in the LA-dorsal ITC pathway in vitro resulted in heightened freezing behavior in mice, supporting the critical roles of D4R-dependent LTD in limiting the expression of fear. Finally, we explored LTD in the context of a mouse model of PTSD (Kaouane et al., 2012) and discovered impairment of LTD at the dorsal ITC.

Our findings indicate that synaptic plasticity at the dorsal ITC serves to actively limit the expression of learned fear and that its impairment may contribute to pathophysiology of PTSD. These data provide new insights into functional roles of a specific inhibitory circuit in the amygdala, which serves to demarcate the range of emotional stimuli that can be retained as long-term memory.

RESULTS

LTD Induction in the Dorsal ITC Synapses after Weak Fear Conditioning

The dorsal ITC receives glutamatergic inputs from the LA and the medial prefrontal cortex (mPFC), which adjust fear responses (Cho et al., 2013; Duvarci and Pare, 2014). We have identified the dorsal ITC neurons spatially and morphologically (Figure 1A; Marowsky et al., 2005). To assess synaptic properties in the LA-dorsal ITC pathway and other neuronal features, we obtained whole-cell patch recordings of excitatory postsynaptic potentials (EPSPs) while stimulating LA (Figure 1B; Table S1). We induced STDP by applying 80 pairs of presynaptic stimulations and postsynaptic action potentials with various time intervals from EPSP initiation (Shin et al., 2006). Interestingly, long-term potentiation (LTP) arose at +4- and +6-ms interval delays in the presence of the $GABA_A$ receptor antagonist picrotoxin, but not in the absence of picrotoxin (Figure S1A). These data suggest that GABAergic transmission tightly regulates STDP in the dorsal ITC neurons as in the BLA neurons (Rodríguez Manzanares et al., 2005; Makkar et al., 2010).

To analyze the behavioral and physiological consequences of different fear-conditioning protocols, we carried out Pavlovian fear conditioning by pairing a tone with either a sub-threshold (0.4 mA for 0.5 s, weak fear conditioning) or a supra-threshold US (0.8 mA for 0.5 s, strong fear conditioning). Weak fear conditioning resulted in reduced levels of freezing at 24 hr after acquisition, which further decayed over the course of several days, comparable to those of the unpaired CS-US or the tone-only control groups (Figure S1B). In contrast, strong fear conditioning led to significantly greater levels of freezing that remained elevated throughout the same time period (Figure S1B). Thus, the weak fear conditioning seems to entail less-salient experience that could not be retained as long-lasting memory. Importantly, LTD was induced in the dorsal ITC neurons by the same STDP protocol in the absence of picrotoxin (+6-ms interval at which GABAergic regulation was maximally effective for the induction of synaptic plasticity; Figure S1A) in the amygdala slices prepared 24 hr after weak fear conditioning (Figure 1C). However, we failed to detect any significant synaptic plasticity in slices from the animals that had undergone either strong fear conditioning or no training (naive) (Figure 1C).

Although we elicited the synaptic responses in the dorsal ITC neurons by stimulation of LA, the possible existence of *en passant* synapses projecting from the mPFC might have obscured which pathway expressed LTD. To further assess synaptic plasticity in distinct pathways, we infused adeno-associated virus (AAV) encoding channelrhodopsin-2 and enhanced yellow fluorescence protein (eYFP) (rAAV5-CamKIIα-hChR2-eYFP) into the LA or mPFC and then validated ChR2 expression with least retrograde infection (Figures 1D and S1C–S1E). After the monosynaptic nature of optogenetically induced EPSPs was verified (Figure S1F), we applied STDP-like optical stimuli. LTD was readily induced by the repeated pairing of light-elicited EPSPs and action potentials after weak fear conditioning when rAAV5-CamKIIα-hChR2-eYFP was infused into LA, but not when it was infused into the mPFC (Figures 1E, S1G, and S1H). The optical STDP also produced no synaptic plasticity in the amygdala slices prepared from naive animals or animals that underwent strong fear conditioning (Figure 1E). Therefore, LTD was induced at the synaptic connections from the LA to the dorsal ITC after weak fear conditioning.

Increased Inhibition to Dorsal ITC Neurons after Weak Fear Conditioning

We monitored basal synaptic transmission and found that miniature IPSCs (mIPSCs) significantly increased after weak fear conditioning (Figures 2A and S2A), whereas no significant change in miniature EPSCs (mEPSCs) was observed despite apparent reduction of excitatory transmission (Figures 2B and S2B). We also evoked disynaptic inhibitory postsynaptic potentials (IPSPs) in dorsal ITC neurons, because they receive GABAergic inputs from neighboring ITC neurons and glutamatergic inputs from the LA (Geracitano et al., 2007; Busti et al., 2011). We observed biphasic PSPs, which consist of fast EPSP and slow IPSP, evoked by LA stimulation and confirmed the disynaptic nature by applying DNQX, an antagonist for α-amino-3-hydroxy-5-methyl-4-isoxazolepropionic acid (AMPA) and kainate receptors (Figure 2C). The input-output curves revealed that the inhibitory drives to the dorsal ITC neurons significantly increased after weak fear conditioning compared with those in other groups (Figure 2D). Thus, GABAergic inputs onto the dorsal ITC neurons might become enhanced by weak fear conditioning and thereby may contribute to the induction of LTD by shunting inhibition (Nishiyama et al., 2010; Talathi et al., 2010). To examine whether neuronal activity

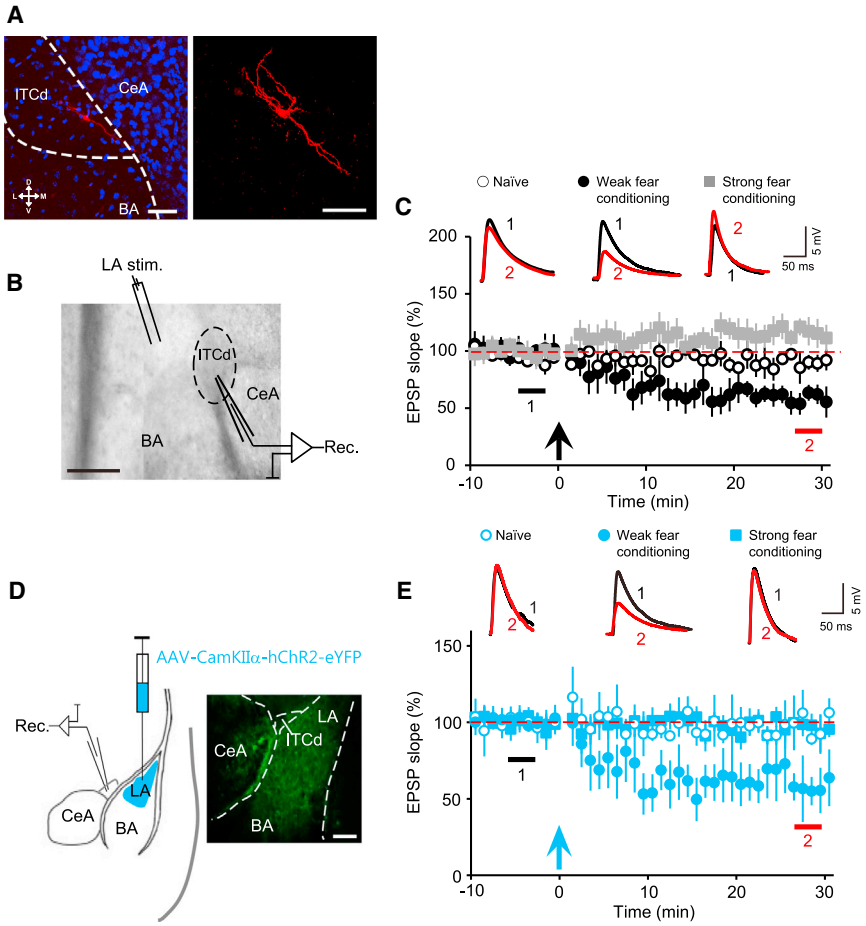

Figure 1. Synaptic Plasticity of the Dorsal ITC Synapses Controlled by Fear Conditioning

(A) Representative images of a neuron that was recorded and labeled with neurobiotin. Left: a merged image of neurobiotin (red) and DAPI staining (blue). The dorsal ITC (ITCd), basal amygdala (BA), and CeA are outlined with white dotted lines. Scale bar, 100 μm. Right: a magnified fluorescence image. Scale bar, 50 μm.

(B) A schematic diagram showing the recording configuration. A whole-cell patch clamp was placed on the dorsal ITC neurons while a stimulating electrode was placed on the LA. LA, ITCd, BA, and CeA, as well as the placement of electrodes, are indicated on a differential interference contrast image. Scale bar, 200 μm.

(C) Synaptic plasticity was assessed with an application of the STDP protocol (+6 ms interval delay) 24 hr after fear conditioning using either sub-threshold (0.4 mA, weak fear conditioning) or supra-threshold US (0.8 mA, strong fear conditioning). The STDP stimulation (a vertical black arrow) induced LTD when sub-threshold US (weak fear conditioning, 60.11% ± 8.91%, N = 6, n = 8, $p < 0.001$, Wilcoxon test) was used for fear conditioning but yielded no significant synaptic plasticity when the animals underwent fear conditioning with supra-threshold US (strong fear conditioning, 115.57% ± 11.06%, N = 6, n = 7, $p > 0.1$, Wilcoxon test) or none (naive, 95.44% ± 8.87%, N = 6, n = 10, $p > 0.1$, Wilcoxon test). Inserts: representative traces with color-matched time points.

(D) A schematic diagram of optogenetic examination of the pathway exhibiting LTD (left). The expression of ChR2 was verified with eYFP (green) mainly in the LA area (right). Scale bar, 100 μm.

(E) Synaptic plasticity in the LA-dorsal ITC pathway was assessed with STDP-like light illumination (a vertical blue arrow) 24 hr after weak fear conditioning (61.95% ± 15.56%, N = 4, n = 5, $p < 0.001$, Wilcoxon test) or strong fear conditioning (96.95% ± 7.68%, N = 4, n = 4, $p > 0.1$, Wilcoxon test). Naive animals were also tested (97.45% ± 10.00%, $p > 0.1$, N = 3, n = 4, $p > 0.1$, Wilcoxon test). Inserts: representative traces with color-matched time points.

Data are presented as mean ± SEM. See also Figure S1 and Table S1.

of the dorsal ITC could be upregulated, we attempted to analyze the spontaneous activity in vivo before and after weak fear conditioning. To this end, we carefully defined the dorsal ITC neurons with their responses to electrical stimulation of the infralimbic regions of the mPFC of live animals and then confirmed the recording sites within the dorsal ITC through postmortem examination (Figures S2C–S2E; Amir et al., 2011). However, we failed to detect significant changes in single-unit activity of those identified ITC neurons (Figures S2F and S2G), suggesting that neuronal activity of the dorsal ITC itself was not significantly affected by weak fear conditioning.

DA-Dependent LTD by Activation of D4R

Consistent with previous reports (Fuxe et al., 2003; de la Mora et al., 2010), our immunohistochemistry data revealed that the dorsal ITC possessed axonal processes intensely labeled with tyrosine hydroxylase, a marker of dopaminergic neurons (Figure S3A). To address possible roles of DA in the dorsal ITC neurons, we analyzed their intrinsic properties in the presence of DA (30 μM). Although it was previously reported that DA itself could alter intrinsic features of ITC neurons (Marowsky et al., 2005), we detected only negligible changes in the resting membrane potentials (RMPs) and excitability before and after DA application (Figures S3B and S3C). The cause for this discrepancy is unclear, but it might be due to age differences of recordings of postnatal day 17 (P17) (Marowsky et al., 2005) versus P56 cells, the different availability of spontaneous GABAergic synaptic transmission, or the further decreased RMPs (approximately −85 mV) in our study. While bath application of DA alone did not alter synaptic transmission (Figure S3D), LTD was readily induced by the STDP protocol in the presence of DA (30 μM) (Figures 3A, S3E, and S3F). To specify the pathway expressing DA-dependent LTD (DA-LTD), we infused rAAV5-CamKIIα-hChR2-eYFP into LA and then were able to induce DA-LTD with photostimulation (Figure 3B). These results support the idea that DA enables the synapses between the LA and dorsal ITC to undergo LTD, which is similar to what we had observed with LTD after weak fear conditioning.

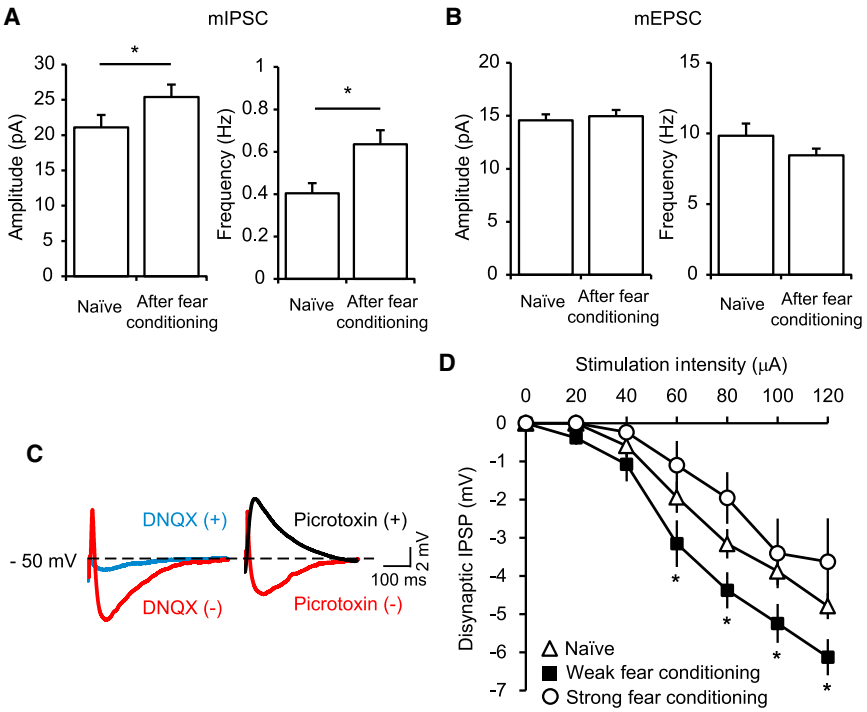

Figure 2. Enhanced Inhibition to the Dorsal ITC Neurons after Weak Fear Conditioning

(A) Both mIPSC amplitude (naive, 21.09 ± 1.75 pA, N = 6, n = 30; after fear conditioning, 25.39 ± 1.77 pA, N = 7, n = 27) and frequency (naive, 0.4 ± 0.05 Hz, N = 6, n = 30; after fear conditioning, 0.63 ± 0.07 Hz, N = 7, n = 27) significantly increased 24 hr after weak fear conditioning (*$p < 0.05$, Mann-Whitney *U* test).

(B) Neither mEPSC amplitude (naive, 14.57 ± 0.57 pA, N = 6, n = 24; after fear conditioning, 14.96 ± 0.58 pA, N = 4, n = 30) nor frequency (naive, 9.84 ± 0.86 Hz, N = 6, n = 24; after fear conditioning, 8.44 ± 0.48 Hz, N = 4, n = 30) was affected by weak fear conditioning ($p > 0.1$, Mann-Whitney *U* test).

(C) Biphasic PSPs were evoked by stimulation of the LA. Both EPSPs and IPSPs were blocked with DNQX (left), while only IPSPs were blocked with picrotoxin (right).

(D) The input-output curves constructed for disynaptic IPSPs show significantly higher feed-forward inhibition after weak fear conditioning, compared to IPSPs after strong fear conditioning or none (naive, N = 6, n = 16; weak fear conditioning, N = 8, n = 13; strong fear conditioning, N = 8, n = 10, *$p < 0.05$, Kruskal-Wallis H test followed by Mann-Whitney *U* test).

Data are presented as mean ± SEM. See also Figure S2.

To identify which subtype of DA receptors plays a dominant role in the induction of DA-LTD, we blocked individual DA receptors with various antagonists in optimal concentrations selective for each receptor (Kwon et al., 2008). Only a D4R-specific antagonist (L-745870) abolished DA-LTD, whereas antagonists of D1/5R (SCH-23390), D2R (L-741626), or D3R (GR-103691) did not affect DA-LTD (Figure 3C). Consistent with the antagonist data, activation of D4R with PD-168077 allowed for the induction of LTD at the dorsal ITC as effectively as DA did, but the agonists for D1/5R (SKF-38393), D2R (quinpirole), or D3R (PD-128907) did not (Figure 3D). To exclude possible cross-reactivity of the pharmacological manipulation, we took advantage of a genetic model deficient in D4R. In D4R knockout (KO) mice, the same STDP protocol could not induce LTD despite the presence of DA (Figure 3E). Importantly, L-745870 also interfered with the induction of LTD that had been normally induced after weak fear conditioning in wild-type (WT) mice, supporting the involvement of D4R (Figure 3F). Taken together, D4R is a major subtype of DA receptors required for the induction of DA-LTD, and its activation is likely to permit LTD in the dorsal ITC after weak fear conditioning.

D4R is expressed throughout brain regions including the amygdala (Oak et al., 2000), and the polymorphisms are implicated in various psychiatric disorders (López León et al., 2005; Shaw et al., 2007). Indeed, our immunohistochemistry revealed the presence of D4R in the dorsal ITC as well as other amygdala nuclei (Figures S3G and S3H). We also used structured illumination microscopy (SIM) over the dorsal ITC neurons to resolve co-localization of D4R with either synaptophysin, a marker for synaptic vesicles, or gephyrin, a marker for GABAergic postsynaptic density. This superresolution imaging indicated that D4R exhibited higher co-localization with synaptophysin than with gephyrin (Figures S3I–S3K). To analyze the subcellular localization of D4R, we performed post-embedding immuno-gold transmission electron microscopy. We detected D4R-bound gold particles in axon terminals of symmetric inhibitory synapses that were labeled with GAD67 and contacting the somas (Figure 3G). In contrast, no D4R immunoreactivity was observed in GAD67-containing presynaptic terminals of D4R KO mice (Figure 3H), as expected. Therefore, D4R appears to be present in the dorsal ITC synapses and predominantly distributed in GABAergic presynaptic terminals.

Feed-Forward Inhibition in the Dorsal ITC Leads to DA-LTD

To elucidate the mechanistic bases of DA-LTD, we monitored basal transmission of the dorsal ITC synapses. After the induction of DA-LTD, mIPSC frequency significantly increased, whereas mEPSCs were unaffected (Figures 4A and 4B). Interestingly, cumulative probability plots of mIPSCs revealed that both frequency and amplitude increased after DA-LTD, but those of mEPSCs did not change (Figures S4A and S4B). We also detected significant increases in disynaptic IPSPs after DA-LTD induction (Figure 4C), indicating enhanced feed-forward inhibition presumably from the neighboring dorsal ITC neurons (Geracitano et al., 2007). To corroborate an increase in GABAergic transmission within the dorsal ITC, we recorded postsynaptic currents (PSCs) from single ITC neurons while interleaving stimulation of LA or dorsal ITC areas (every 5 s) (Figure 4D). Due to the small size of the dorsal ITC, monosynaptic IPSCs were evoked

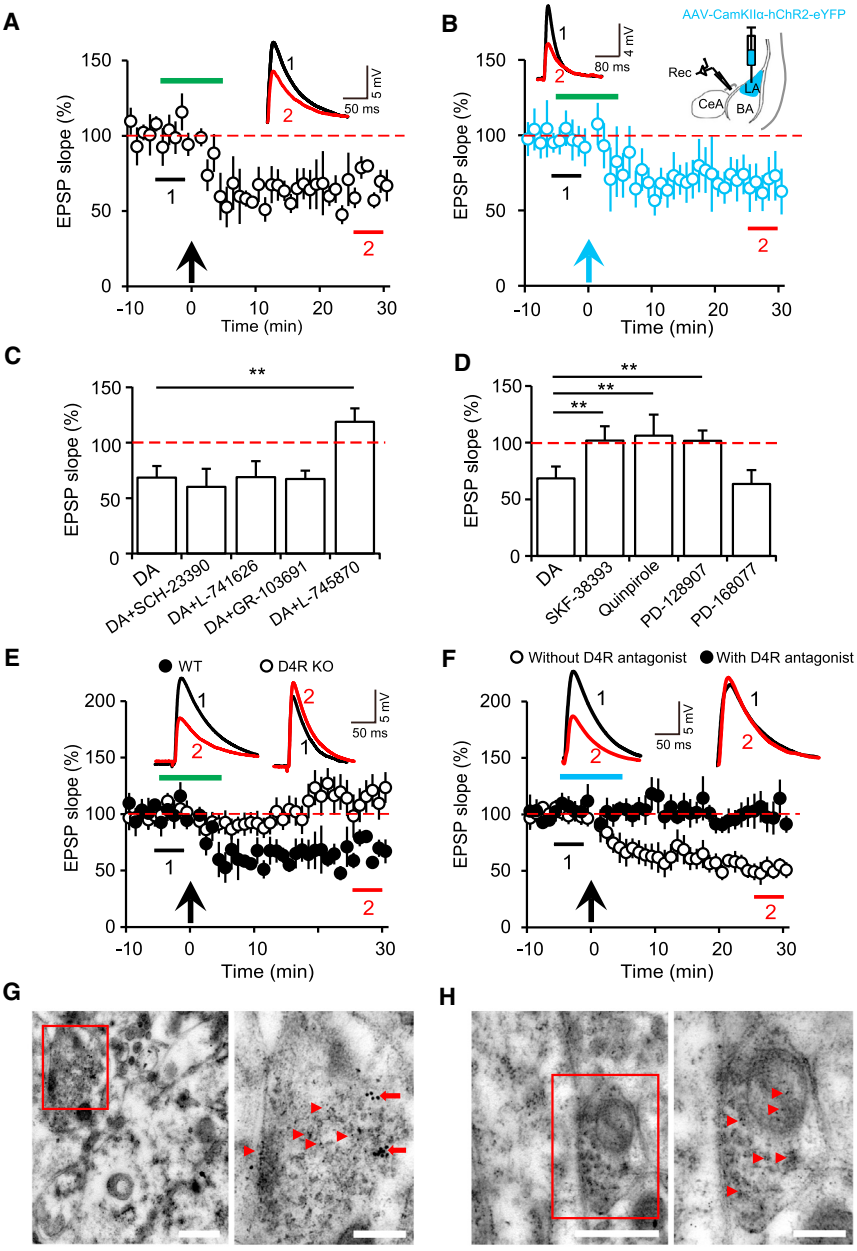

Figure 3. D4R-Dependent LTD in the Dorsal ITC Synapses

(A) DA treatment (a green bar) during STDP stimulation (a vertical black arrow) resulted in LTD at the dorsal ITC (65.79% ± 9.39%, N = 6, n = 10, $p < 0.001$, Wilcoxon test). Inserts: representative traces with color-matched time points.

(B) After rAAV5-CamKIIα-hChR2-eYFP was infused into LA, LTD was induced by repeated light illumination (a vertical blue arrow) in the presence of DA (a green bar) (68.52% ± 13.57%, N = 6, n = 7, $p < 0.001$, Wilcoxon test). Inserts: representative traces with color-matched time points (left) and a schematic diagram (right).

(C) DA-LTD was assessed using subtype-specific DA receptor antagonists (30 μM DA, 68.56% ± 10.47%, N = 6, n = 7; DA + 5 μM SCH-23390, 60.07% ± 16.41%, N = 5, n = 5; DA + 200 nM L-741626, 68.92% ± 14.47%, N = 4, n = 6; DA + 50 nM GR-103691, 67.34% ± 7.46%, N = 4, n = 6; DA + 50 nM L-745870, 118.94% ± 12.07%, N = 6, n = 8. **$p < 0.01$, Kruskal-Wallis H test followed by Mann-Whitney *U* test).

(D) DA-LTD was assessed using subtype-specific DA receptor agonists (30 μM DA, 67.37 ± 9.46%, N = 6, n = 6; 10 μM SKF-38393, 101.74% ± 12.64%, N = 4, n = 5; 100 nM quinpirole, 106.61% ± 18.62%, N = 5, n = 7; 200 nM PD-128907, 101.74% ± 8.96%, N = 5, n = 6; 200 nM PD-168077, 63.47% ± 12.28%, N = 7, n = 10. **$p < 0.01$, Kruskal-Wallis H test followed by Mann-Whitney *U* test).

(E) DA-LTD was not induced in D4R KO mice (D4R KO, 115.26% ± 15.38%, N = 4, n = 7, $p > 0.1$; WT, 68.52% ± 13.57%, N = 5, n = 6, $p < 0.001$, Wilcoxon test). Insert: representative trace with color-matched time points. Duration of DA treatment is depicted with a green bar and the application of STDP protocol is denoted with a vertical black arrow.

(F) While LTD was readily induced after weak fear conditioning (without D4R antagonist, 60.11% ± 8.91%, N = 5, n = 7, $p < 0.001$, Wilcoxon test), D4R antagonist (50 μM L-745870, a blue bar) precluded LTD induction (with D4R antagonist, 99.98% ± 12.56%, N = 6, n = 7. $p > 0.1$, Wilcoxon test). The application of STDP protocol is denoted with a vertical black arrow. Inserts: representative traces with color-matched time points.

(G) Immuno-electron microscopic images showing the subcellular localization of D4R and GAD67 at the dorsal ITC of WT mice. The area outlined with a red box (left) is magnified to delineate a presynaptic terminal (right). Arrows and arrowheads denote D4R-immunogold particle (12 nm) and GAD67-immunogold particles (6 nm), respectively. Scale bars represent 500 nm (left) and 200 nm (right).

(H) Immuno-electron microscopic images of D4R KO mice. The area outlined with a red box (left) is magnified to delineate a presynaptic terminal (right). We detected no large gold particles for D4R, but only GAD67 (+) particles (6 nm). Scale bars represent 500 nm (left) and 200 nm (right).

Data are presented as mean ± SEM. See also Figure S3.

with glass electrodes, whereas EPSCs were evoked by stimulating the LA with standard metal electrodes. Notably, the latencies of postsynaptic currents evoked by stimulation of both the LA (2.78 ± 0.19 ms) and the dorsal ITC (3.76 ± 0.17 ms) were consistent with latencies of previously reported monosynaptic currents (Cho et al., 2013; Felix-Ortiz et al., 2013). Once DA-LTD was induced, IPSCs were potentiated while EPSCs were depressed (Figure 4E). Presynaptic neurotransmitter release can be represented by the quantal content proportional to the inverse square of the coefficient of variation ($1/CV^2$) of evoked responses (Malinow and Tsien, 1990). Consistent with the enhanced presynaptic release of GABA, $1/CV^2$ increased for IPSCs, but not for EPSCs (Figure S4C).

After synaptically coupled ITC neurons were identified with action potentials elicited by current injection and resultant outward IPSCs, we analyzed the unitary IPSCs (uIPSCs) by paired

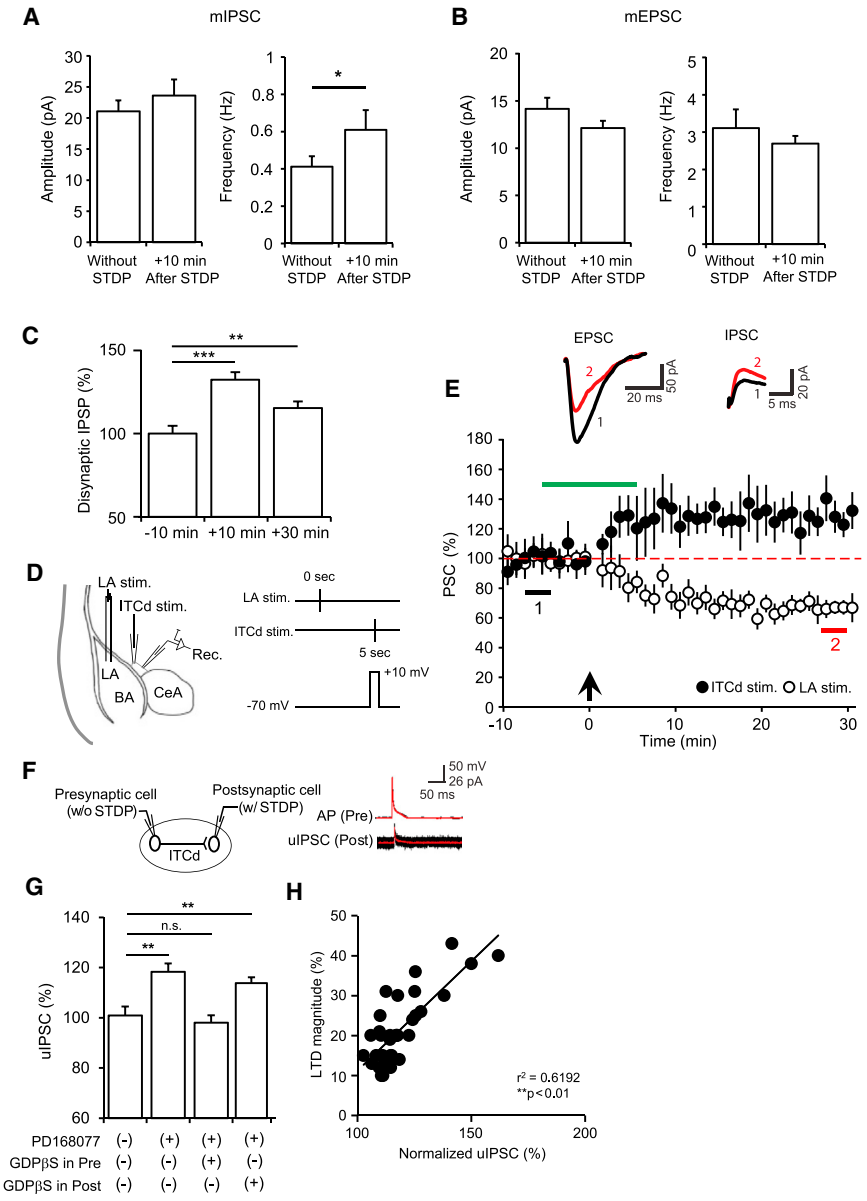

Figure 4. Feed-Forward Inhibition Increased by DA-LTD

(A) mIPSC frequency (without STDP, 0.41 ± 0.06 Hz; +10 min after STDP, N = 6, n = 24, 0.61 ± 0.11 Hz, N = 6, n = 27, *p < 0.05, Mann-Whitney *U* test), but not amplitude (amplitude: without STDP, 21.08 ± 1.75 pA, N = 6, n = 24; +10 min after STDP, 23.62 ± 2.6 pA, N = 6, n = 27, p > 0.1, Mann-Whitney *U* test), increased upon the induction of DA-LTD.

(B) DA-LTD did not affect mEPSC amplitude (without STDP, 14.15 ± 1.18 pA, N = 6, n = 14; +10 min after STDP, 12.12 ± 0.78 pA, N = 6, n = 18) or frequency (frequency: without STDP, 3.11 ± 0.50 Hz, N = 6, n = 14; +10 min after STDP, 2.69 ± 0.21 Hz, N = 6, n = 18, p > 0.1 for all, Mann-Whitney *U* test).

(C) Disynaptic IPSPs increased concomitantly to the induction of DA-LTD relative to its own baseline at −10 min (N = 5, n = 14, p < 0.001, repeated-measures ANOVA; +10 min, 134.4% ± 4.4%, ***p < 0.001; +30 min, 115.4% ± 3.9%, **p < 0.01, post hoc Bonferroni test).

(D) Synaptic responses from the dorsal ITC neurons obtained by interleaved stimulation of LA and the dorsal ITC. A schematic diagram depicting positions of electrodes (left) and a timeline of each stimulus for PSC recordings (right).

(E) When DA-LTD was induced, IPSCs were significantly potentiated, but EPSCs were depressed (ITC stimulation, 127.95% ± 12.5%; LA stimulation, 66.80% ± 6.65%; N = 3, n = 6, p < 0.01 for both PSCs, Wilcoxon test). Duration of DA treatment is depicted with a green bar and the application of STDP protocol is denoted with a vertical black arrow. Inserts: representative traces with color-matched time points.

(F) A schematic diagram of a paired whole-cell recording (left). Sample traces of single action potentials (APs) given to a presynaptic neuron and the elicited unitary IPSCs (uIPSCs) at the postsynaptic cell recorded at the holding potential of −40 mV (right: red, average traces; black, individual traces). Note that the STDP stimulation was applied by injecting current to postsynaptic neurons, but not presynaptic neurons, while stimulating the LA.

(G) uIPSCs from postsynaptic neurons were significantly increased after the induction of D4R-dependent LTD, compared with the corresponding baselines (PD-168077 (−), 100.98% ± 3.58%, N = 3, n = 5; PD-168077 (+), 118.28% ± 3.35%, N = 4, n = 12, **p < 0.01, Kruskal-Wallis H test followed by Mann-Whitney *U* test). During the induction of D4R-dependent LTD, GDPβS was included in recording pipettes for the dorsal ITC neurons (GDPβS in pre, 98.7% ± 1.96%, N = 5, n = 15, p > 0.05; GDPβS in post, 113.28% ± 1.27%, N = 6, n = 17, **p < 0.01; Kruskal-Wallis H test followed by Mann-Whitney U test, relative to the PD-168077 (−) group).

(H) Correlation of normalized uIPSCs and the magnitude of DA-LTD (N = 11, n = 32, r^2 = 0.6192, **p < 0.01, Pearson's correlation coefficient).

Data are presented as mean ± SEM. See also Figure S4.

recording (Figure 4F). The amplitude of uIPSCs markedly increased when LTD was induced by injecting currents to the postsynaptic ITC neurons while stimulating the LA in the presence of PD-168077 (Figure 4G). Notably, the increase in the amplitude of uIPSCs was positively correlated with LTD magnitude, consistent with the causal role of GABA release for LTD (Figure 4H). Since D4R was enriched at presynaptic sites (Figure 3G), we asked: does the increment of GABA release resulting from activation of presynaptic D4R contribute to LTD? To address this question, we selectively included GDPβS, an antagonist of G protein signaling in either presynaptic or postsynaptic ITC neurons. GDPβS blocked an LTD-induced increment of uIPSC amplitude when infused into the presynaptic ITC neurons, but not when infused into the postsynaptic ITC neurons (Figure 4G). Collectively, DA-LTD arose from the potentiation of GABAergic transmission in intrinsic circuits of the dorsal ITC, most likely by activation of presynaptic D4R.

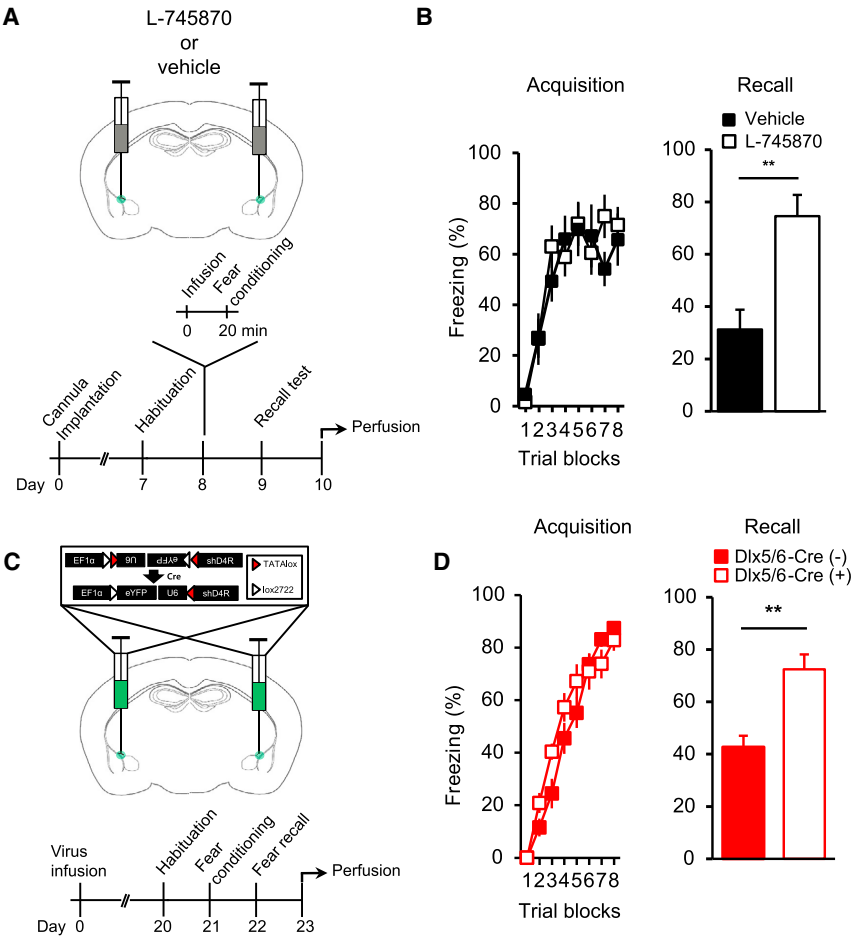

Figure 5. Freezing Behavior Regulated by D4R Activity in Dorsal ITC Neurons

(A) An experimental scheme (top) and a timeline (bottom) for a D4R antagonist infusion and behavioral tests. Freezing behavior was assessed after weak fear conditioning when either L-745870 or vehicle was infused to the region centered around the dorsal ITC areas bilaterally.

(B) Following drug infusion through cannulae, we measured freezing levels during fear acquisition (left) and tested fear recall 24 hr after weak fear conditioning (right) (vehicle, 31.25% ± 7.56%, N = 8; L-745870, 74.55% ± 8.10%, N = 9, $^{**}p < 0.01$, Mann-Whitney *U* test).

(C) The schematic sequence of cKD-eYFP-shD4R (top) and a timeline for virus infusion and behavioral tests (bottom) are depicted. The Cre-dependent inversion resulted in simultaneous expression of eYFP and shRNA for D4R in the dorsal ITC of *Dlx5/6-Cre* (+) mice. Freezing behavior was assessed after weak fear conditioning when D4R was depleted in the region centered around the dorsal ITC area.

(D) We measured freezing levels during fear acquisition (left) and tested fear recall 24 hr after weak fear conditioning (right: *Dlx5/6-Cre* (−), 42.75% ± 4.26%, N = 7; *Dlx5/6-Cre* (+), 72.47% ± 5.66%, N = 9, $^{**}p < 0.01$, Mann-Whitney *U* test).

Data are presented as mean ± SEM. See also Figure S5 and Supplemental Experimental Procedures.

Blockade of D4R or Reversal of LTD Is Sufficient to Increase the Expression of Fear

If DA-LTD at the dorsal ITC is a synaptic mechanism that regulates neural circuits conveying fear memory, manipulation of D4R activity or synaptic plasticity at the dorsal ITC should affect fear memory. To test this hypothesis, we first examined the behavioral consequences of DA-LTD by pharmacological inactivation of D4R at the dorsal ITC. We injected either vehicle or L-745870 bilaterally into the dorsal ITC areas (Figures S5A and S5B) and then assessed acquisition and expression of fear memory (Figure 5A). Animals that received either vehicle or L-745870 displayed comparable freezing levels during acquisition, which increased as the pairings of CS and US were repeatedly presented (Figure 5B). When assessed at 24 hr after weak fear conditioning, L-745870-infused mice exhibited significantly higher levels of freezing compared with vehicle-infused animals (Figure 5B), indicating the involvement of D4R activity for fear expression. We next developed a new genetic method to deplete D4R in GABAergic neurons of the dorsal ITC. This viral vector enables us to knock down a given gene with small hairpin RNA (shRNA) and simultaneously identify those infected/knocked-down neurons with expression of eYFP in a Cre-dependent manner (Figures S5C and S5D; see Supplemental Experimental Procedures for detailed information). We infused the AAV containing shRNA for D4R (rAAV2-cKD-eYFP-shD4R) into the dorsal ITC of *Dlx5/6-Cre* (−) or *Dlx5/6-Cre* (+) mice expressing Cre at GABAergic neurons (Figures 5C and S5E–S5G). eYFP was expressed mainly in the dorsal ITC area (Figures S5G and S5H), and D4R was markedly depleted in the dorsal ITC of *Dlx5/6-Cre* (+) mice compared to that of *Dlx5/6-Cre* (−) controls (Figure S5I). Importantly, *Dlx5/6-Cre* (+) mice that received rAAV2-cKD-eYFP-shD4R displayed higher levels of freezing than *Dlx5/6-Cre* (−) mice, whereas freezing levels during the acquisition of fear memory were indistinguishable (Figure 5D). Interestingly, WT and D4R KO mice did not differ in fear expression to weak fear conditioning (data not shown), highlighting the importance of the dorsal ITC circuits for controlling fear expression. The small size of the dorsal ITC makes it difficult to be completely certain that we localized the region-specific knockdown of D4R only to the dorsal ITC. However, it should be noted that we employed both pharmacological and genetic approaches for local manipulation of D4R with the same results. Therefore, we provide evidence that D4R in the dorsal ITC neurons could, at least in part, be a functional prerequisite for limiting fear expression, especially to less-salient experience, and thus might delineate the integrity of fear memory.

If synaptic plasticity in the dorsal ITC circuit was faithfully induced by the cues associated with weak fear conditioning, fear recall by cue exposure prior to recordings would affect the subsequent induction of LTD. Indeed, LTD was occluded when CS-induced recall was given to the fear-conditioned mice

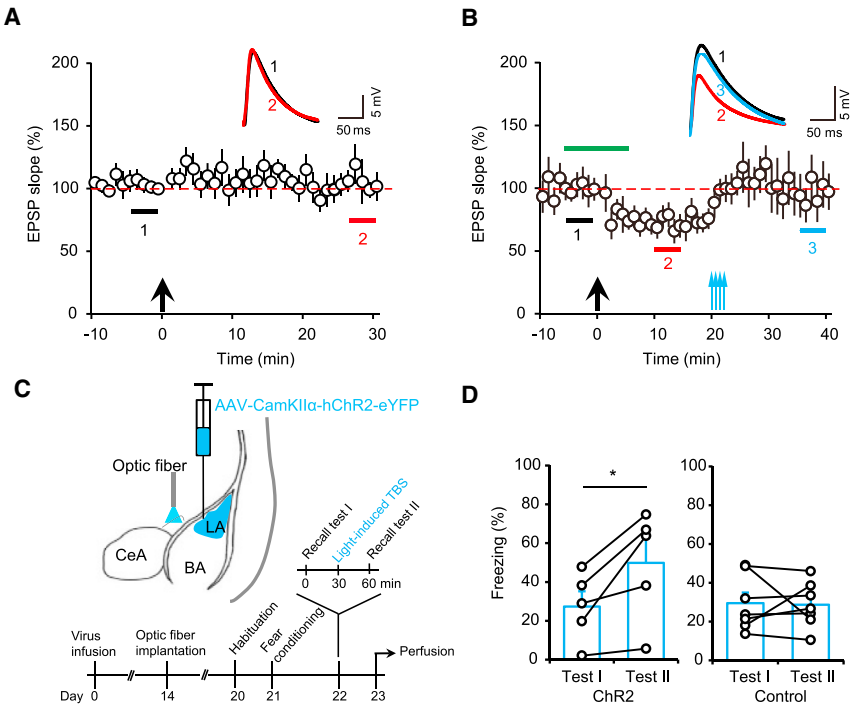

Figure 6. Optogenetic Reversal of LTD Leading to Heightened Expression of Fear Memory

(A) Occlusion of LTD at the dorsal ITC by prior fear recall. Acute brain slices were made 1 hr after the cue-induced fear recall (102.37% ± 7.85%, N = 4, n = 7, $p > 0.1$, Wilcoxon test). The application of STDP protocol is denoted with a vertical black arrow. Inserts: representative traces with color-matched time points.

(B) Validation of reversal of DA-LTD by optogenetic TBS-like stimulation. On the amygdala slices prepared from the animals that received rAAV5-CamKIIα-hChR2-eYFP, DA-LTD was induced electrically and then examined with an application of light illumination mimicking TBS. The optogenetic TBS (blue arrows) abrogated DA-LTD and thereby restored strength of synaptic transmission to the baseline levels (+10 min, 75.21% ± 9.69%, $p < 0.05$; +40 min, 97.57% ± 17.06%; N = 4, n = 7, $p > 0.1$; Wilcoxon test). Duration of DA treatment is depicted with a green bar and the application of STDP protocol is denoted with a vertical black arrow. Inserts: representative traces with color-matched time points.

(C) A schematic diagram for in vivo optogenetic manipulation (top) and a timeline for behavioral tests (bottom) are depicted. After recovery from the implantation of optic fibers targeting right above the dorsal ITC area, the animals underwent weak fear conditioning, and then freezing levels to the same conditioned cue were measured before and after the optogenetic TBS.

(D) Optogenetic TBS onto the region centered on the dorsal ITC was sufficient to increase freezing levels in the animals that received rAAV5-CamKIIα-hChR2-eYFP in the LA area (left: test I, 27.32% ± 7.87%; test II, 49.81% ± 12.64%, N = 5, *$p < 0.05$, Wilcoxon test), but not in control-virus-infused animals (right: test I, 29.52% ± 5.44%; test II, 28.70% ± 4.46%, N = 7, $p > 0.1$, Wilcoxon test).

Data are presented as mean ± SEM. See also Figure S6.

(Figure 6A). We surmised that fear expression could be altered if LTD is reversed in the LA-dorsal ITC pathway. We sought to optogenetically manipulate the LA-dorsal ITC pathway in order to abrogate LTD that normally arose after weak fear conditioning. In the amygdala slices from WT mice that received rAAV5-CamKIIα-hChR2-eYFP in LA, DA-LTD was abrogated by repeated light illumination mimicking theta burst stimulation (TBS) (Figure 6B). It was shown that TBS induced *N*-methyl-D-aspartic acid receptor (NMDAR)-dependent LTP in the LA-dorsal ITC pathway (Huang et al., 2014). We explored how optical TBS could affect DA-LTD and discovered that TBS-induced reversal of LTD also depended on NMDAR activity using its antagonist, 2-amino-5-phosphonopentanoic acid (APV) (Figure S6A). With optic fibers implanted at the top of the dorsal ITC, we applied optogenetic TBS and detected increased activity of the dorsal ITC neurons (Figures S6B–S6D). When the optogenetic TBS was applied between fear recall tests (Figure 6C), rAAV5-CamKIIα-hChR2-eYFP-infused mice displayed significant increases in freezing levels to the conditioned cue in the second recall test compared to those in the first test, whereas optogenetic TBS resulted in no behavioral changes in rAAV5-CamKIIα-eYFP-infused mice (Figure 6D). Although our ex vivo recordings did not allow us to precisely determine how much the given fear recall could depress the strength of the dorsal ITC synapses, LTD at the dorsal ITC would be a critical cellular substrate that can limit learned fear.

Impaired LTD at the Dorsal ITC in a PTSD-like Animal Model

Since both D4R blockade and reversal of LTD resulted in increased levels of fear expression, LTD could be affected in the dorsal ITC of PTSD models. While most of the animal models for PTSD have been produced by exposure to a variety of stresses (Pitman et al., 2012), PTSD models can also be produced by administration of glucocorticoids (Kaouane et al., 2012). The PTSD-like impairment of fear memory could be represented with enhanced fear responses as well as incapability to discriminate between threat- and safeness-predicting stimuli (Kaouane et al., 2012). When we injected corticosterone (CORT; 5 mg/kg), a predominant form of glucocorticoid, into mice that underwent weak fear conditioning, PTSD-like impairment in fear memory was obviously observed; 24 hr after weak fear conditioning, the conditioned cue resulted in higher freezing levels in CORT-injected mice than in vehicle-injected animals, regardless of pairing the sub-threshold US with either the auditory cue or context (Figure 7A). Importantly, the context also increased freezing levels in CORT-injected mice although they underwent only cue conditioning (Figure 7B). Subsequent to verification of PTSD-like impairment of fear memory in CORT-injected mice, we found that LTD could not be triggered in the dorsal ITC of CORT-treated mice, regardless of fear conditioning, whereas LTD was readily induced in vehicle-treated mice (Figures 7C and S7A). Interestingly, a glucocorticoid receptor

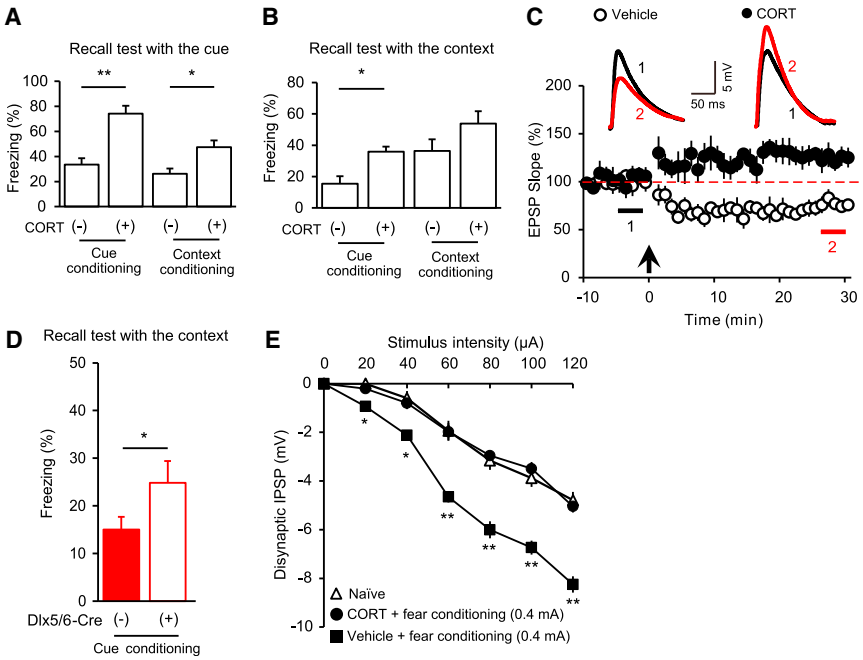

Figure 7. Impaired LTD at the Dorsal ITC of the Animal Exhibiting PTSD-like Behavior

(A) Cue-induced freezing was measured in vehicle- or CORT-injected mice that had undergone either cue or context conditioning (cue conditioning: vehicle, 33.55% ± 5.02%, N = 6; CORT, 74.19% ± 6.23%, N = 7, **p < 0.01; context conditioning: vehicle, 26.25% ± 4.01%, N = 10; CORT, 47.49% ± 5.36%, N = 10, *p < 0.05, Mann-Whitney *U* test).

(B) Context-induced freezing was measured in vehicle- or CORT-injected mice that had undergone either cue or context conditioning (cue conditioning: vehicle, 15.43% ± 4.74%, N = 6; CORT, 35.94% ± 3.19%, N = 8, *p < 0.05; context conditioning: vehicle, 36.31% ± 7.41%, N = 10; CORT, 53.81% ± 7.84%, N = 10, p > 0.05, Mann-Whitney *U* test).

(C) In CORT-injected animals, STDP stimulation failed to induce LTD, but resulted in modest LTP at the dorsal ITC, after weak fear conditioning (vehicle, 73.46% ± 6.55%, N = 5, n = 4, p < 0.001; CORT, 126.06% ± 10.91%, N = 6, n = 5, p < 0.05, Wilcoxon test). Inserts: representative traces with color-matched time points. The application of STDP protocol is denoted with a vertical black arrow.

(D) Cue-conditioned *Dlx5/6-Cre* (+) mice that had received rAAV2-cKD-eYFP-shD4R bilaterally in the regions centered around the dorsal ITC areas exhibited higher freezing levels when subjected to the context, compared with freezing behavior exhibited by control *Dlx5/6-Cre* (–) mice (*Dlx5/6-Cre* (–), 14.92% ± 2.68%, N = 7; *Dlx5/6-Cre* (+), 25.17% ± 3.77%, N = 6, *p < 0.05, Mann-Whitney *U* test).

(E) Input-output curves of disynaptic IPSPs after the application of STDP protocol. Disynaptic IPSPs did not differ between CORT-injected and naive mice, whereas they were significantly increased in the mice that had undergone only weak fear conditioning without CORT (naive, N = 8, n = 16; CORT + fear conditioning, N = 7, n = 7; vehicle + fear conditioning, N = 7, n = 6, **p < 0.01, Kruskal-Wallis H test followed by Mann-Whitney *U* test).

Data are presented as mean ± SEM. See also Figure S7.

antagonist RU38486 blocked both DA-LTD in naive mice and LTD in mice that underwent weak fear conditioning (Figures S7B and S7C). These results prompted us to speculate that D4R elicits downstream signaling pathway(s) of glucocorticoid receptors. Consistent with functional overlapping of CORT- and D4R-triggered signaling, irrelevant context led to increased freezing levels in *Dlx5/6-Cre* (+) mice in which D4R was depleted in the dorsal ITC, compared with those in *Dlx5/6-Cre* (–) mice (Figure 7D). To obtain mechanistic insights into the LTD impairment, we constructed the input-output curves of evoked disynaptic IPSPs. The disynaptic IPSPs in CORT-treated mice were not altered after weak fear conditioning, whereas those in vehicle-treated mice significantly increased (Figure 7E). Thus, the LTD deficit in CORT-treated mice appears to result from the impaired augmentation of inhibitory inputs to the dorsal ITC neurons. Altogether, these data suggest that abnormality in D4R-mediated signaling and/or defective synaptic plasticity of the amygdala inhibitory circuit contribute(s) to PTSD-like memory impairment.

DISCUSSION

We here provide evidence that the amygdala inhibitory pathway undergoes synaptic plasticity, which, in turn, modulates the expression of fear memory. These results are based on a multidisciplinary approach involving electrophysiological and behavioral experiments using pharmacological, genetic, and optogenetic manipulations. Although we are confident that our electrophysiological analyses were specific for the LA-dorsal ITC synapses, given the small size of the dorsal ITC, it is possible that our pharmacological and optogenetic manipulations of D4R might not be completely selective for the dorsal ITC neurons and thereby would have affected neighboring regions. Nevertheless, our combined electrophysiological and behavioral data support the idea that the synaptic modulation in the amygdala inhibitory circuit centered on the dorsal ITC is one of underlying mechanisms that deter less-salient experience from entering long-term memory storage, and its deficit could potentially contribute to fear-related psychiatric diseases such as PTSD.

DA-Dependent Synaptic Plasticity at the Dorsal ITC upon Exposure to Less-Salient Experience

It has been long believed that less- or non-salient experience cannot initiate the signaling cascade sufficiently to induce synaptic plasticity in the relevant circuits of the amygdala (Rogerson et al., 2014). Contrary to this notion, we found that LTD was induced in the LA-dorsal ITC pathway by electrical or optogenetic STDP stimulation after weak fear conditioning that had normally caused negligible fear responses in the subsequent test days. Importantly, LTD induced at excitatory synapses resulted from augmented GABAergic inputs impinging onto the dorsal ITC neurons. The physiological relevance of this synaptic plasticity induced by specific behavioral manipulation and STDP could be recapitulated by DA-LTD, considering that STDP was causally modulated by the levels of DA (Figure S3F).

While DA is generally recognized for its importance in reward learning, motivation, and attention (Schultz, 2002), DA also has emerged as a neuromodulator for fear-related learning (Fadok et al., 2009; Bromberg-Martin et al., 2010). For instance, stressful events increase the activity of dopaminergic neurons leading to enhanced release of DA, which in turn could mediate behavioral adaptation to the outcome-predicting cues (Ventura et al., 2007). It has been proposed that the saliency of aversive experience would correlatively set DA concentrations (Wang and Tsien, 2011). If this were the case for fear memory, weak fear conditioning would increase the concentration of DA to an appropriate level that would allow for the induction of LTD, whereas strong fear conditioning would not. Thus, this heterosynaptic LTD could be a cellular mechanism whereby less-salient experience is prevented from being stored as long-term memory.

Although it remains unclear why LTD could not be induced after strong fear conditioning, the different binding affinities of each subtype of DA receptors might account for this interesting observation. D4R has been known to have a higher binding affinity to DA than D1R (Sunahara et al., 1991; Van Tol et al., 1991). Activation of D1R can result in reduction of inhibitory outputs from ITC neurons (Marowsky et al., 2005). Accordingly, the amount of DA released by weak fear conditioning could activate D4R only, but strong fear conditioning would raise the DA level high enough to activate D1R additionally, leading to reversal of LTD by normalizing GABA release. Indeed, we found that a D1/5R antagonist, SCH-23390, rescued LTD after strong fear conditioning (Figure S4E). These data suggest that, at least in part, D1R activity can abrogate LTD upon exposure to salient experience, although we could not exclude possible involvement of other cellular mechanisms such as differential expression level or trafficking of each DA receptor in response to given experience. However, because in vivo DA levels and individual DA receptors have not been measured and carefully assessed, respectively, at the amygdala or the dorsal ITC following specific fear conditioning, these possibilities should be clarified with subsequent studies.

D4R-Mediated Regulation of Inhibitory Circuits of the Amygdala

In contrast to the classical views for inhibitory roles of D2-like receptors (Missale et al., 1998; Neves et al., 2002), activation of D4R enriched at presynaptic terminals causes, paradoxically, an increase in GABA release. However, the DA-induced increase in GABA release was also observed in the previous reports that D2-like receptors affect excitability of cortical pyramidal neurons through regulation of the local interneurons (Tseng and O'Donnell, 2004, 2007; Zhong and Yan, 2014). We have extensively corroborated the presynaptic attributes of D4R for LTD with superresolution and electron microscopy as well as with paired-recordings following selective blockade of G protein signaling. These data clearly indicate that presynaptic D4R in the dorsal ITC neurons plays a major role in controlling the expression of fear memory. However, we also observed a significant amount of D4R present in the postsynaptic sites of the dorsal ITC neurons and in the neighboring amygdala regions such as the basal nucleus of the amygdala and CeA. Although the physiological roles of D4R in those areas remain unclear, it may well be involved in trafficking of AMPARs (Yuen and Yan, 2009) or regulation of NMDARs (Martina and Bergeron, 2008). It is unlikely, however, that D4R participates in the induction of DA-LTD that we have observed.

Although it was recently reported that sensory inputs to the dorsal ITC undergo fear-learning-related changes in a presynaptic $GABA_B$ receptor-dependent manner (Asede et al., 2015), DA-LTD in the LA-dorsal ITC pathway was not affected by the blockade of $GABA_B$ receptors (Figure S4I), suggesting that GABA can exert shunting effects on excitatory transmission mainly via $GABA_A$ receptors (Nishiyama et al., 2010; Talathi et al., 2010). Interestingly, in our study, the dorsal ITC neurons displayed slightly more hyperpolarized RMPs, compared to those of the previous report (Marowsky et al., 2005), which might account for the negligible levels of DA-triggered and K^+-induced hyperpolarization, because RMPs that we have observed are close to the K^+ equilibrium potential (Geracitano et al., 2007). Nevertheless, DA-LTD in the dorsal ITC is independent of alteration in intrinsic membrane properties but relies on $GABA_A$ receptor activity.

Medially localized ITCs including the dorsal and ventral ITCs are topographically polarized in a lateromedial direction and form an inhibitory interface controlling the trafficking of synaptic signals from the BLA to CeA (Royer et al., 1999; Palomares-Castillo et al., 2012). Given the decreases in excitatory transmission and concomitant increases in inhibitory transmission, our LTD data suggest the existence of complex inhibitory-disinhibitory interactions between dorsal ITC neurons. Moreover, mean firing rates that remained unaltered by the application of weak fear conditioning (Figure S2) could be attributed to occurrence of heterogeneous synaptic dynamics among the dorsal ITC neurons that have been predicted to be critical for the computational role of the amygdala in fear learning (Geracitano et al., 2007). Furthermore, the dorsal ITC provides feed-forward inhibition to CeA, mainly to its lateral sector, which in turn causes disinhibition of the medial sector of the CeA (Royer et al., 1999; Pare and Duvarci, 2012; Duvarci and Pare, 2014). Impairment or reversal of D4R-mediated LTD at the dorsal ITC might result in abnormal activation of the medial sector of the CeA, which facilitates even less-salient information to elicit fear-related behavior. D4R has previously been shown to modulate inhibitory circuits and play a role in learning and recall of salient versus non-salient emotional information (Baimoukhametova et al., 2004; Lauzon et al., 2009). Taken together, D4R-dependent synaptic plasticity in the inhibitory circuit is one of critical regulators for controlling the expression of fear memory, although possible cellular heterogeneity and output preference of ITC neurons also can participate in adjustment of individual pathways.

Relevance of LTD at the Dorsal ITC to PTSD

Although the cellular and molecular mechanisms leading to PTSD are just beginning to be explored, PTSD is thought to be due to dysfunction in the suppression of fear to non-relevant cues or extinction of learned fear (Layton and Krikorian, 2002; Myers and Davis, 2007). Glucocorticoids released by the adrenal glands facilitate and enhance formation and maintenance of the stress-related memory, which would contribute to occurrence and progression of PTSD (van Zuiden et al., 2012; Labonté et al., 2014). Indeed, the animals that received CORT displayed PTSD-like memory impairment as previously demonstrated (Kaouane et al., 2012). The lack of LTD at the dorsal ITC of CORT-injected mice supports the idea that synaptic plasticity in the dorsal ITC circuit

serves a discriminative role that suppresses the expression of irrelevantly excessive and overgeneralized fear response to cues that remind less-salient experience. Given that CORT both increased the excitability of principal neurons and reduced the $GABA_A$ receptor-mediated IPSPs in the amygdala (Duvarci and Paré, 2007), CORT treatment might result in a decrease in GABA release from the dorsal ITC neurons as well, which affects LTD in their downstream ITC neurons. This leads us to suggest that maladaptation of GABAergic signaling and the resultant LTD impairment at the dorsal ITC would contribute, at least in part, to endophenotypes of PTSD such as heightened fear responses.

EXPERIMENTAL PROCEDURES

See Supplemental Experimental Procedures for full experimental procedures.

Subjects and Surgery

Male 8- to 10-week-old mice were used. All procedures for animal experiments were approved by the ethical review committee of POSTECH and performed in accordance with the relevant guidelines. For AAV infection, viral solution was infused into each hemisphere in coordinates targeting the LA, mPFC, or dorsal ITC. For drug infusion, cannulae were implanted bilaterally, targeting the dorsal ITC. Optic fiber was implanted to target above the dorsal ITC areas for in vivo optogenetic manipulation.

Behavioral Tests

For fear conditioning, mice were conditioned with auditory tones that co-terminated with electric foot shocks. The pairs of stimuli were presented with pseudo-random inter-trial intervals. Recall of learned fear memory was tested by exposure to the CS for 2 min. Freezing behavior was measured during the presentation of CS.

Viral Vectors

rAAV5-CamKIIα-hChR2-eYFP and rAAV5-CamKIIα-eYFP were obtained from Vector Core of University of North Carolina and used for optogenetic manipulation. For conditional knockdown experiments, rAAV2 was designed and produced as previously described (Hommel et al., 2003).

Electrophysiology

Acute coronal slices were prepared from 8-week-old male mice. Using whole-cell recording, STDP was induced by applying 80 pairs of presynaptic stimulations and postsynaptic action potentials (Shin et al., 2006). In vivo spontaneous firings from the dorsal ITC neurons were monitored using tungsten wires after the dorsal ITC neurons were identified as previously described (Amir et al., 2011).

Statistics

Statistical tests, statistical significance, and the numbers animals used (N) and/or experiments performed (n) are specified in the figure legends. All reported values are mean ± SEM, and the statistical significance is indicated with "n.s." (non-significant) or asterisks.

SUPPLEMENTAL INFORMATION

Supplemental information includes Supplemental Experimental Procedures, seven figures, and one table and can be found with this article online at http://dx.doi.org/10.1016/j.neuron.2015.09.001.

AUTHOR CONTRIBUTIONS

O.-B.K., E.R.K. and J.-H.K. conceived experiments. O.-B.K. and M.-J.J. performed electrophysiology. Seungho Lee, H.-J.J. and J.H.L. made stereotaxic surgery and behavioral assays. H.J.K., S.C., J.H.L., and B.K. conducted imaging studies including SIM and electron microscopy. Sanghyeon Lee developed and produced conditional knockdown AAV. S.-J.K. and S.K.P. did biochemical assays and immunocytochemistry. O.-B.K., J.H.L., Y.-B.C, and J.-H.K. did data analysis. J.H.L., Y.-B.C., C.H.B., E.R.K., and J.-H.K. wrote the manuscript.

ACKNOWLEDGMENTS

We thank K. Deisseroth for pAAV-EF1a-DIO-eYFP construct and B. Kang for electron microscopy analysis. We also thank B.-K. Kaang and V. Bolshakov for critical reading. We appreciate M. Poo for constructive discussions and advice throughout this study. We thank J.-H. Han for in vivo recording. This work was supported by grants from the National Research Foundation of Korea (2014051826, 2015M3C7A1027351, and 2014R1A2A2A01002921) and Korea Healthcare Technology R&D Project (A111284) to J.-H.K.

Received: December 25, 2014
Revised: May 19, 2015
Accepted: August 17, 2015
Published: September 24, 2015

REFERENCES

Amano, T., Unal, C.T., and Paré, D. (2010). Synaptic correlates of fear extinction in the amygdala. Nat. Neurosci. *13*, 489–494.

Amir, A., Amano, T., and Pare, D. (2011). Physiological identification and infralimbic responsiveness of rat intercalated amygdala neurons. J. Neurophysiol. *105*, 3054–3066.

Asede, D., Bosch, D., Lüthi, A., Ferraguti, F., and Ehrlich, I. (2015). Sensory inputs to intercalated cells provide fear-learning modulated inhibition to the basolateral amygdala. Neuron *86*, 541–554.

Baimoukhametova, D.V., Hewitt, S.A., Sank, C.A., and Bains, J.S. (2004). Dopamine modulates use-dependent plasticity of inhibitory synapses. J. Neurosci. *24*, 5162–5171.

Bissière, S., Humeau, Y., and Lüthi, A. (2003). Dopamine gates LTP induction in lateral amygdala by suppressing feedforward inhibition. Nat. Neurosci. *6*, 587–592.

Bromberg-Martin, E.S., Matsumoto, M., and Hikosaka, O. (2010). Dopamine in motivational control: rewarding, aversive, and alerting. Neuron *68*, 815–834.

Busti, D., Geracitano, R., Whittle, N., Dalezios, Y., Mańko, M., Kaufmann, W., Sätzler, K., Singewald, N., Capogna, M., and Ferraguti, F. (2011). Different fear states engage distinct networks within the intercalated cell clusters of the amygdala. J. Neurosci. *31*, 5131–5144.

Cho, J.-H., Deisseroth, K., and Bolshakov, V.Y. (2013). Synaptic encoding of fear extinction in mPFC-amygdala circuits. Neuron *80*, 1491–1507.

de la Mora, M.P., Gallegos-Cari, A., Arizmendi-García, Y., Marcellino, D., and Fuxe, K. (2010). Role of dopamine receptor mechanisms in the amygdaloid modulation of fear and anxiety: Structural and functional analysis. Prog. Neurobiol. *90*, 198–216.

Duvarci, S., and Paré, D. (2007). Glucocorticoids enhance the excitability of principal basolateral amygdala neurons. J. Neurosci. *27*, 4482–4491.

Duvarci, S., and Pare, D. (2014). Amygdala microcircuits controlling learned fear. Neuron *82*, 966–980.

Ehrlich, I., Humeau, Y., Grenier, F., Ciocchi, S., Herry, C., and Lüthi, A. (2009). Amygdala inhibitory circuits and the control of fear memory. Neuron *62*, 757–771.

Fadok, J.P., Dickerson, T.M.K., and Palmiter, R.D. (2009). Dopamine is necessary for cue-dependent fear conditioning. J. Neurosci. *29*, 11089–11097.

Felix-Ortiz, A.C., Beyeler, A., Seo, C., Leppla, C.A., Wildes, C.P., and Tye, K.M. (2013). BLA to vHPC inputs modulate anxiety-related behaviors. Neuron *79*, 658–664.

Fuxe, K., Jacobsen, K.X., Höistad, M., Tinner, B., Jansson, A., Staines, W.A., and Agnati, L.F. (2003). The dopamine D1 receptor-rich main and paracapsular intercalated nerve cell groups of the rat amygdala: relationship to the dopamine innervation. Neuroscience *119*, 733–746.

Geracitano, R., Kaufmann, W.A., Szabo, G., Ferraguti, F., and Capogna, M. (2007). Synaptic heterogeneity between mouse paracapsular intercalated neurons of the amygdala. J. Physiol. *585*, 117–134.

Hommel, J.D., Sears, R.M., Georgescu, D., Simmons, D.L., and DiLeone, R.J. (2003). Local gene knockdown in the brain using viral-mediated RNA interference. Nat. Med. *9*, 1539–1544.

Huang, C.C., Chen, C.C., Liang, Y.C., and Hsu, K.S. (2014). Long-term potentiation at excitatory synaptic inputs to the intercalated cell masses of the amygdala. Int. J. Neuropsychopharmacol. *17*, 1233–1242.

Jüngling, K., Seidenbecher, T., Sosulina, L., Lesting, J., Sangha, S., Clark, S.D., Okamura, N., Duangdao, D.M., Xu, Y.L., Reinscheid, R.K., and Pape, H.C. (2008). Neuropeptide S-mediated control of fear expression and extinction: role of intercalated GABAergic neurons in the amygdala. Neuron *59*, 298–310.

Kaouane, N., Porte, Y., Vallée, M., Brayda-Bruno, L., Mons, N., Calandreau, L., Marighetto, A., Piazza, P.V., and Desmedt, A. (2012). Glucocorticoids can induce PTSD-like memory impairments in mice. Science *335*, 1510–1513.

Kwon, O.-B., Paredes, D., Gonzalez, C.M., Neddens, J., Hernandez, L., Vullhorst, D., and Buonanno, A. (2008). Neuregulin-1 regulates LTP at CA1 hippocampal synapses through activation of dopamine D4 receptors. Proc. Natl. Acad. Sci. USA *105*, 15587–15592.

Labonté, B., Azoulay, N., Yerko, V., Turecki, G., and Brunet, A. (2014). Epigenetic modulation of glucocorticoid receptors in posttraumatic stress disorder. Transl. Psychiatry *4*, e368.

Lauzon, N.M., Bishop, S.F., and Laviolette, S.R. (2009). Dopamine D1 versus D4 receptors differentially modulate the encoding of salient versus nonsalient emotional information in the medial prefrontal cortex. J. Neurosci. *29*, 4836–4845.

Layton, B., and Krikorian, R. (2002). Memory mechanisms in posttraumatic stress disorder. J. Neuropsychiatry Clin. Neurosci. *14*, 254–261.

Lee, S., Kim, S.-J., Kwon, O.-B., Lee, J.H., and Kim, J.-H. (2013). Inhibitory networks of the amygdala for emotional memory. Front. Neural Circuits *7*, 129.

Likhtik, E., Popa, D., Apergis-Schoute, J., Fidacaro, G.A., and Paré, D. (2008). Amygdala intercalated neurons are required for expression of fear extinction. Nature *454*, 642–645.

López León, S., Croes, E.A., Sayed-Tabatabaei, F.A., Claes, S., Van Broeckhoven, C., and van Duijn, C.M. (2005). The dopamine D4 receptor gene 48-base-pair-repeat polymorphism and mood disorders: a meta-analysis. Biol. Psychiatry *57*, 999–1003.

Makkar, S.R., Zhang, S.Q., and Cranney, J. (2010). Behavioral and neural analysis of GABA in the acquisition, consolidation, reconsolidation, and extinction of fear memory. Neuropsychopharmacology *35*, 1625–1652.

Malinow, R., and Tsien, R.W. (1990). Presynaptic enhancement shown by whole-cell recordings of long-term potentiation in hippocampal slices. Nature *346*, 177–180.

Marowsky, A., Yanagawa, Y., Obata, K., and Vogt, K.E. (2005). A specialized subclass of interneurons mediates dopaminergic facilitation of amygdala function. Neuron *48*, 1025–1037.

Martina, M., and Bergeron, R. (2008). D1 and D4 dopaminergic receptor interplay mediates coincident G protein-independent and dependent regulation of glutamate NMDA receptors in the lateral amygdala. J. Neurochem. *106*, 2421–2435.

Missale, C., Nash, S.R., Robinson, S.W., Jaber, M., and Caron, M.G. (1998). Dopamine receptors: from structure to function. Physiol. Rev. *78*, 189–225.

Myers, K.M., and Davis, M. (2007). Mechanisms of fear extinction. Mol. Psychiatry *12*, 120–150.

Neves, S.R., Ram, P.T., and Iyengar, R. (2002). G protein pathways. Science *296*, 1636–1639.

Nishiyama, M., Togashi, K., Aihara, T., and Hong, K. (2010). GABAergic activities control spike timing- and frequency-dependent long-term depression at hippocampal excitatory synapses. Front. Synaptic Neurosci. *2*, 22.

Oak, J.N., Oldenhof, J., and Van Tol, H.H. (2000). The dopamine D(4) receptor: one decade of research. Eur. J. Pharmacol. *405*, 303–327.

Palomares-Castillo, E., Hernández-Pérez, O.R., Pérez-Carrera, D., Crespo-Ramírez, M., Fuxe, K., and Pérez de la Mora, M. (2012). The intercalated paracapsular islands as a module for integration of signals regulating anxiety in the amygdala. Brain Res. *1476*, 211–234.

Pare, D., and Duvarci, S. (2012). Amygdala microcircuits mediating fear expression and extinction. Curr. Opin. Neurobiol. *22*, 717–723.

Pitman, R.K., Rasmusson, A.M., Koenen, K.C., Shin, L.M., Orr, S.P., Gilbertson, M.W., Milad, M.R., and Liberzon, I. (2012). Biological studies of post-traumatic stress disorder. Nat. Rev. Neurosci. *13*, 769–787.

Rodríguez Manzanares, P.A., Isoardi, N.A., Carrer, H.F., and Molina, V.A. (2005). Previous stress facilitates fear memory, attenuates GABAergic inhibition, and increases synaptic plasticity in the rat basolateral amygdala. J. Neurosci. *25*, 8725–8734.

Rogan, M.T., Stäubli, U.V., and LeDoux, J.E. (1997). Fear conditioning induces associative long-term potentiation in the amygdala. Nature *390*, 604–607.

Rogerson, T., Cai, D.J., Frank, A., Sano, Y., Shobe, J., Lopez-Aranda, M.F., and Silva, A.J. (2014). Synaptic tagging during memory allocation. Nat. Rev. Neurosci. *15*, 157–169.

Rosenkranz, J.A., and Grace, A.A. (2002). Dopamine-mediated modulation of odour-evoked amygdala potentials during pavlovian conditioning. Nature *417*, 282–287.

Royer, S., Martina, M., and Paré, D. (1999). An inhibitory interface gates impulse traffic between the input and output stations of the amygdala. J. Neurosci. *19*, 10575–10583.

Schultz, W. (2002). Getting formal with dopamine and reward. Neuron *36*, 241–263.

Shaw, P., Gornick, M., Lerch, J., Addington, A., Seal, J., Greenstein, D., Sharp, W., Evans, A., Giedd, J.N., Castellanos, F.X., and Rapoport, J.L. (2007). Polymorphisms of the dopamine D4 receptor, clinical outcome, and cortical structure in attention-deficit/hyperactivity disorder. Arch. Gen. Psychiatry *64*, 921–931.

Shin, R.-M., Tsvetkov, E., and Bolshakov, V.Y. (2006). Spatiotemporal asymmetry of associative synaptic plasticity in fear conditioning pathways. Neuron *52*, 883–896.

Sunahara, R.K., Guan, H.C., O'Dowd, B.F., Seeman, P., Laurier, L.G., Ng, G., George, S.R., Torchia, J., Van Tol, H.H., and Niznik, H.B. (1991). Cloning of the gene for a human dopamine D5 receptor with higher affinity for dopamine than D1. Nature *350*, 614–619.

Talathi, S.S., Hwang, D.U., Carney, P.R., and Ditto, W.L. (2010). Synchrony with shunting inhibition in a feedforward inhibitory network. J. Comput. Neurosci. *28*, 305–321.

Tseng, K.Y., and O'Donnell, P. (2004). Dopamine-glutamate interactions controlling prefrontal cortical pyramidal cell excitability involve multiple signaling mechanisms. J. Neurosci. *24*, 5131–5139.

Tseng, K.Y., and O'Donnell, P. (2007). Dopamine modulation of prefrontal cortical interneurons changes during adolescence. Cereb. Cortex *17*, 1235–1240.

Van Tol, H.H., Bunzow, J.R., Guan, H.C., Sunahara, R.K., Seeman, P., Niznik, H.B., and Civelli, O. (1991). Cloning of the gene for a human dopamine D4 receptor with high affinity for the antipsychotic clozapine. Nature *350*, 610–614.

van Zuiden, M., Geuze, E., Willemen, H.L.D.M., Vermetten, E., Maas, M., Amarouchi, K., Kavelaars, A., and Heijnen, C.J. (2012). Glucocorticoid receptor pathway components predict posttraumatic stress disorder symptom development: a prospective study. Biol. Psychiatry *71*, 309–316.

Ventura, R., Morrone, C., and Puglisi-Allegra, S. (2007). Prefrontal/accumbal catecholamine system determines motivational salience attribution to both reward- and aversion-related stimuli. Proc. Natl. Acad. Sci. USA *104*, 5181–5186.

Wang, D.V., and Tsien, J.Z. (2011). Convergent processing of both positive and negative motivational signals by the VTA dopamine neuronal populations. PLoS ONE *6*, e17047.

Yuen, E.Y., and Yan, Z. (2009). Dopamine D_4 receptors regulate AMPA receptor trafficking and glutamatergic transmission in GABAergic interneurons of prefrontal cortex. J. Neurosci. *29*, 550–562.

Zhong, P., and Yan, Z. (2014). Distinct physiological effects of dopamine D4 receptors on prefrontal cortical pyramidal neurons and fast-spiking interneurons. Cereb. Cortex. Published online August 21, 2014. http://dx.doi.org/10.1093/cercor/bhu190.

Neuron

Supplemental Information

Dopamine Regulation of Amygdala Inhibitory Circuits for Expression of Learned Fear

Oh-Bin Kwon, Joo Han Lee, Hyun Jin Kim, Seungho Lee, Sanghyeon Lee, Min-Jae Jeong, Su-Jeong Kim, Hee-Jung Jo, Bumjin Ko, Sunghoe Chang, Sang Ki Park, Yun-Beom Choi, Craig H. Bailey, Eric R. Kandel, and Joung-Hun Kim

Supplemental Information

Inventory of Supplemental Information

Table S1, related to Figure 1: Intrinsic features of the dorsal ITCd neurons.

Supplemental Experimental Procedures

Supplemental References

Supplemental Text

Development of a novel viral vector that allows for simultaneous Cre-mediated knock-down and fluorescence labeling

A number of genetic methods including Cre-loxP system have been developed and used to accomplish the cell-type specific expression of given genes, which have tremendously facilitated investigation of functional roles of those genes at the cellular and organism levels (Le Pichon and Chesler, 2014; Ting and Feng, 2014). Although application of Cre-loxP has been heavily used to overexpress genes, it has been much less frequently exploited to achieve the cell-type specific gene silencing (Kasim et al., 2004; Tiscornia et al., 2004; Zhou et al., 2007). The cell-type specific knock-down of given genes could be made using pSico vectors carrying the U6 promoter, CMV-eGFP reporter/stop cassette, and a pair of TATAlox to express small hairpin RNA (shRNA) selective to the target gene (Ventura et al., 2004; Lee et al., 2010; Woo et al., 2012). Cre-mediated recombination of pSico vectors could be represented by removal of CMV-eGFP reporter/stop cassette and the consequential disappearance of the fluorescence signal (Ventura et al., 2004). As a result, pSico vectors do not permit ones to discriminate between non-infected and infected cells where Cre-mediated recombination occurred.

Because of the small size of the dorsal ITC of the amygdala, a genetic method that couples Cre-dependent recombination with Cre-specific expression of reporter protein would be ideal for the identification of the transduced dorsal ITC neurons containing shRNA that can deplete a specific gene. Although the DIO (double floxed inverse open reading frame) construct has been useful for Cre-dependent expression of given genes in a specific type of cells (Atasoy et al., 2008; Sohal et al., 2009), DIO in itself was not ideal for Cre-inducible knock-down because of the palindromic structure of shRNA. By modifying pAAV-EF1a-DIO-eYFP (Sohal et al., 2009), we have developed a viral vector with which transduced cells enabled to express a fluorescence reporter upon the Cre-mediated recombination that results in depletion of a specific gene product. To generate EF1α-DIO-TATAlox-eYFP-U6-shRNA (shRNA-mediated conditional knock-down with eYFP expression, cKD-eYFP-shRNA), loxP sequence was converted to TATAlox, which contained inverted TATAbox, and the U6 promoter was inserted to the 3' end of eYFP (Figure 5C). We also introduced restriction enzyme sites *Hpa*I and *Eco*RI, for shRNA insertion to allow for the optimal 25 base pairs between TATAbox and a

transcription start site (Ventura et al., 2004). Indeed, this construct enabled shRNA to deplete a specific gene in Cre-expressing cells and simultaneously eYFP to be expressed upon Cre-mediated recombination. Therefore, this novel conditional knock-down system would allow us to distinguish the infected neurons from non-infected neurons by expression of eYFP.

To verify the efficacy of Cre-mediated recombination, we first applied rAAV2-EF1α-DIO-TATAlox-eYFP-U6-shD4R containing shRNA for D4R (cKD-eYFP-shD4R) to the mixed culture of normal and Cre-expressing HEK-293 cells. Immunostaining results revealed that eYFP was selectively expressed in Cre-positive cells, but not in Cre-negative cells (Figure S5C), which substantiated the Cre-dependent expression of eYFP. Moreover, we first expressed D4R in either Cre (+) or Cre (-) HEK-293 cells by transfecting pCMV-D4R-turboGFP and then tested whether shD4R could knock down D4R. We found that D4R expression was not affected by cKD-eYFP-shD4R virus in Cre (-) cells, but D4R expression was significantly reduced in Cre (+) cells when infected with virus encoding eYFP and shD4R (Figure S5D). However, the expression of eYFP appeared to be indifferent to expression of D4R or shD4R since eYFP levels did not differ between rAAV2-cKD-eYFP-shD4R- and control rAAV2-cKD-eYFP-infected Cre (+) cells (Figure S5D). Finally, we validated *in vivo* efficacy of cKD-eYFP-shD4R for both Cre-mediated expression of eYFP and D4R depletion. Immunohistochemistry analysis revealed that D4R was depleted selectively in eYFP-expressing dorsal ITC neurons of *Dlx5/6-Cre* (+) mice, but not in neurons of *Dlx5/6-Cre* (-) mice (Figure S5I), with least infection to the other nuclei of the amygdala (Figures S5G-S5I). Using this viral vector, we were able to address the physiological and behavioral consequence of manipulating D4R protein levels mainly in the dorsal ITC neurons without affecting the other types of neurons or neurons outside the dorsal ITC areas (Figures 5D and 7E). Therefore, cKD-eYFP-shRNA could be a valuable resource that allows for labeling the virally-infected neurons without immunostaining, applicable to a number of cell biological and physiological investigations besides this study.

Supplemental Figures

Figure S1.

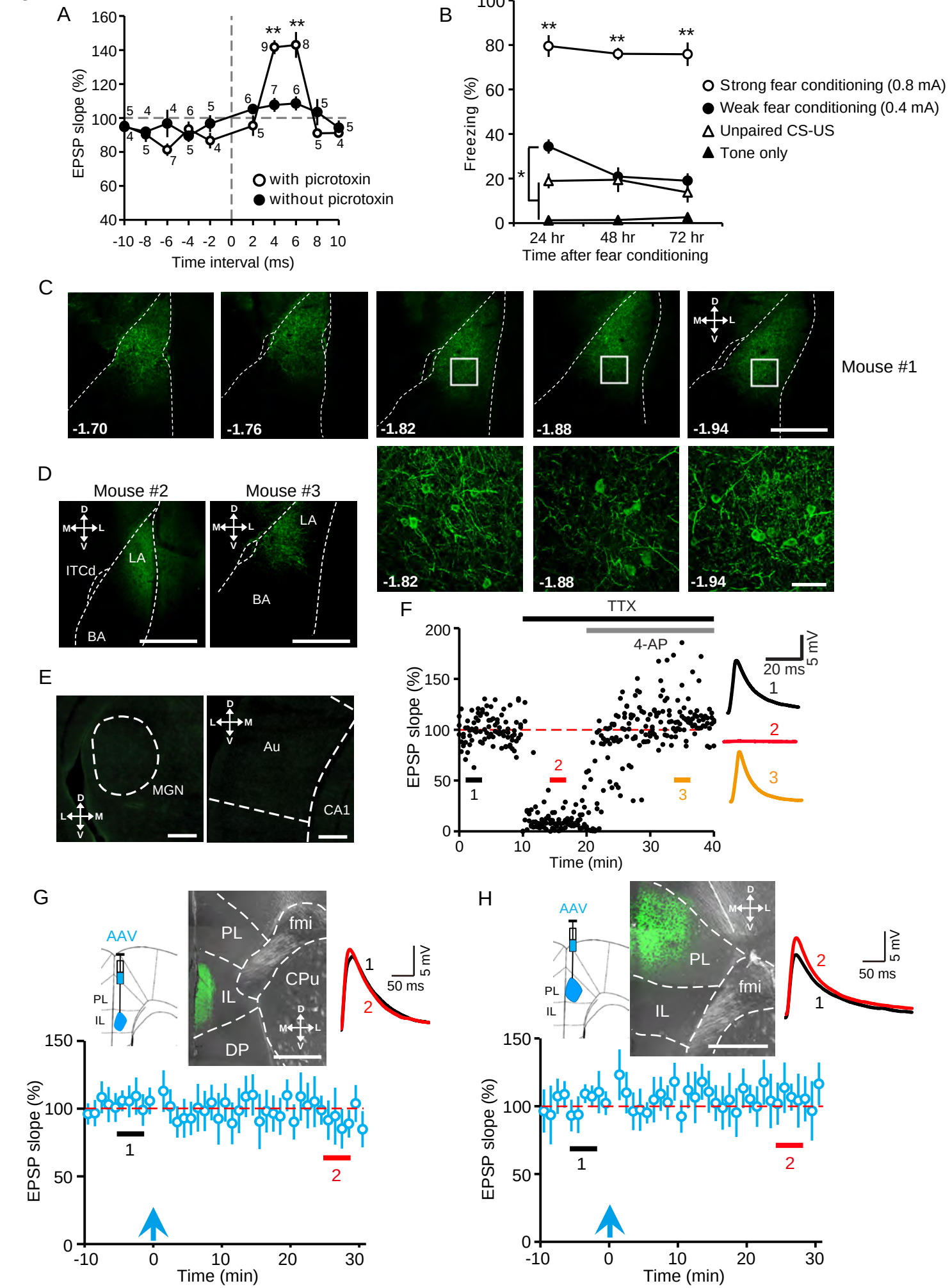

Figure S1, related to Figure 1.

(A) Summary of STDP experiments in the dorsal ITC neurons during LA stimulation. STDP was induced by pairing of presynaptic stimulation (80 EPSPs) with postsynaptic action potentials when either the EPSP preceded the action potential in a postsynaptic neuron (positive time intervals) or the action potential preceded the EPSP (negative time intervals). STDP was tested with or without picrotoxin (100 μM) in the bath solution. The number of cells is indicated for each time interval. At +4 ms and +6 ms, significant changes in EPSPs were observed (**p < 0.01, Mann-Whitney U test).

(B) Freezing responses to the conditioned cue was measured in the ensuing days after the mice were subjected to individual conditioning protocols using either sub-threshold (0.4 mA, N = 6) or supra-threshold US (0.8 mA, N = 7, **p < 0.01 for all time points, Kruskal-Wallis H test followed by Mann-Whitney U test relative to weak fear conditioning group). As controls, freezing responses to the auditory tone were also measured from mice that underwent unpaired conditioning (0.8 mA, N = 7, *p < 0.05 for 24 hours, p > 0.05 for 48 and 72 hours, Kruskal-Wallis H test followed by Mann-Whitney U test relative to weak fear conditioning group) or that had experienced CS alone (N = 5, *p < 0.05 for all, Kruskal-Wallis H test followed by Mann-Whitney U test relative to weak fear conditioning group).

(C) Representative fluorescence images of coronal sections of a mouse, containing LA infected with rAAV5-CamKIIα-hChR2-eYFP. Distances from the bregma (mm) are specified on each image. External and intermediate capsules are delineated with white dotted lines. Highly-magnified Z-stacks of the boxed areas indicate that ChR2-eYFP was expressed in somas and neurites of LA neurons (bottom). Scale bars = 500 μm (top) and 50 μm (bottom).

(D) Representative fluorescence images of coronal sections of two other mice that were infected with rAAV5-CamKIIα-hChR2-eYFP. ChR2-eYFP was mainly expressed in the LA area, but minimally in the basal amygdala (BA). External and intermediate capsules are delineated with white dotted lines. Scale bars = 500 μm.

(E) Coronal sections containing brain regions upstream of LA display negligible fluorescence after infusion of rAAV5-CamKIIα-hChR2-eYFP into LA, arguing against the possibility of retrograde infection. Medial geniculate nucleus (MGN) and primary auditory cortex (Au) are

outlined with white dotted lines. Scale bars = 200 μm.

(F) Monosynaptic nature of optically-elicited EPSPs (N = 2, n = 3) was verified by sequential application of TTX (a black bar, 1 μM) and 4-AP (a gray bar, 400 μM). Representative traces are delineated with color-matched time points (right).

(G) EPSPs were elicited in the IL-dorsal ITC pathway with light pulses and then STDP was assessed with repeated light stimulation (a vertical blue arrow) that mimicked presynaptic stimulation of the STDP protocol, 24 hours after weak fear conditioning (96.37 ± 15.18%, N = 6, n = 7, $p > 0.1$, Wilcoxon test). *Inserts*: A schematic illustration showing rAAV5-CamKIIα-hChR2-eYFP infusion into IL (left, adapted from Franklin and Paxinos, 1997). The expression of ChR2 was confirmed with eYFP signal (middle). Representative traces with color-matched time points are depicted (right). IL, PL, caudate putamen (CPu), dorsal peduncular cortex (DP), and forceps minor of the corpus callosum (fmi) are delineated with white dotted lines. Scale bar = 200 μm.

(H) EPSPs were elicited in the PL-dorsal ITC pathway with light pulses and then STDP was assessed with repeated light stimulation (a vertical blue arrow) that mimicked presynaptic stimulation of the STDP protocol, 24 hours after weak fear conditioning (106.59 ± 17.03 %, N = 6, n = 6, $p > 0.1$, Wilcoxon test). *Inserts*: A schematic illustration showing rAAV5-CamKIIα-hChR2-eYFP infusion into PL (left, adapted from Franklin and Paxinos, 1997). The expression of ChR2 was confirmed with eYFP signal (middle). Representative traces with color-matched time points are depicted (right). IL, PL, and fmi are delineated with white dotted lines. Scale bar = 200 μm.

Data are represented as mean ± SEM.

Figure S2.

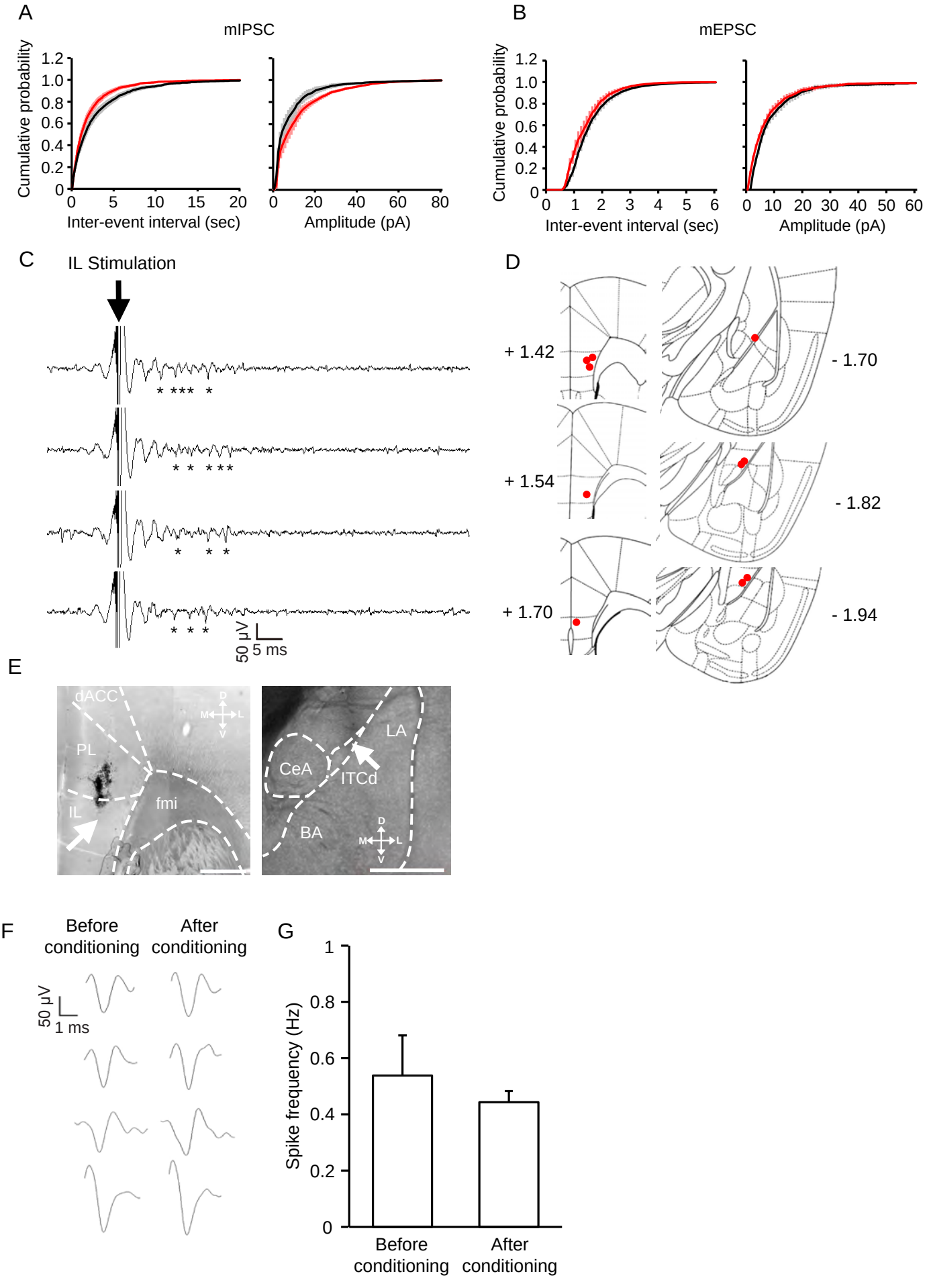
A
mIPSC
Cumulative probability
Inter-event interval (sec)
Amplitude (pA)
B
mEPSC
Cumulative probability
Inter-event interval (sec)
Amplitude (pA)
C
IL Stimulation
50 μV
5 ms
D
+ 1.42
- 1.70
+ 1.54
- 1.82
+ 1.70
- 1.94
E
dACC
PL
IL
fmi
LA
CeA
ITCd
BA
F
Before conditioning
After conditioning
50 μV
1 ms
G
Spike frequency (Hz)
Before conditioning
After conditioning

Figure S2, related to Figure 2.

(A) A cumulative probability plot of mIPSCs from naïve (black) and weak fear conditioning (red) groups (inter-event interval, $p < 0.001$; amplitude, $p < 0.001$, Kolmogorov-Smirnov test). Errors are indicated by shaded bars.

(B) A cumulative probability plot of mEPSCs from naïve (black) and weak fear conditioning (red) groups (inter-event interval, $p > 0.1$; amplitude, $p > 0.1$, Kolmogorov-Smirnov test). Errors are indicated by shaded bars.

(C) Electrical stimulation of IL triggered burst-like responses in the dorsal ITC neurons. Asterisks (*) indicate spikes after stimulus which is denoted by a black arrow. The high-frequency burst could be elicited by IL stimulation only when recording electrodes were placed within the dorsal ITC areas as shown in (D) and (E). Note that the latency and number of evoked spikes are comparable to those previously obtained from the dorsal ITC (Amir et al., 2011).

(D) Histological reconstruction of electrode placements. Schematic illustrations of IL (left) and the dorsal ITC (right) showing the electrode sites (red circles). Distances from the bregma (mm) are indicated. Images are adapted from Franklin and Paxinos, 1997.

(E) Representative DIC images of coronal brain slices for verification of electrode placement. Electrode tips in IL and the dorsal ITC (ITCd) were confirmed during the post-mortem examination. For stimulation sites, IL, PL, the dorsal anterior cingulate cortex (dACC), forceps minor of the corpus callosum (fmi) are delineated with white dotted lines (left). For recording sites, LA, CeA, ITCd, and the basal amygdala (BA) are delineated with white dotted lines (right). The electrode tips are marked with white arrows. Scale bars = 500 μm.

(F) Representative traces of spike waveforms recorded from four isolated units are shown before and after weak fear conditioning.

(G) A summary histogram showing that spontaneous firing rates of the isolated units were not altered by weak fear conditioning ($N = 5$, $n = 13$ units, $p > 0.1$, Wilcoxon test).

Data are represented as mean ± SEM.

Figure S3.

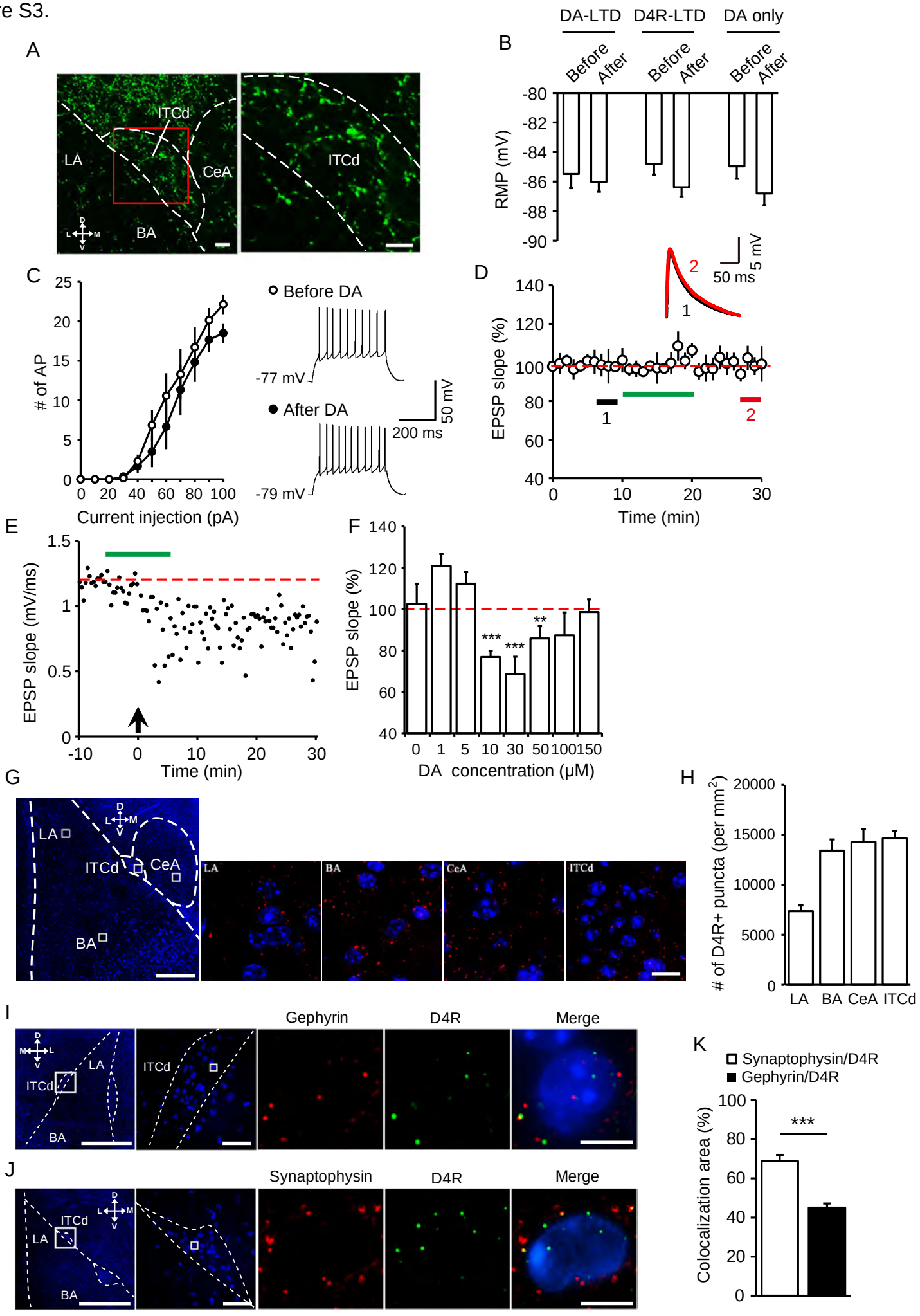
A
ITCd
LA
CeA
BA
ITCd
B
DA-LTD
D4R-LTD
DA only
Before
After
RMP (mV)
C
# of AP
Current injection (pA)
Before DA
After DA
-77 mV
-79 mV
50 mV
200 ms
D
EPSP slope (%)
Time (min)
5 mV
50 ms
E
EPSP slope (mV/ms)
Time (min)
F
EPSP slope (%)
DA concentration (μM)
G
LA
ITCd
CeA
BA
H
# of D4R+ puncta (per mm2)
LA BA CeA ITCd
I
Gephyrin
D4R
Merge
J
Synaptophysin
D4R
Merge
K
Synaptophysin/D4R
Gephyrin/D4R
Colocalization area (%)

Figure S3, related to Figure 3.

(A) Immunostaining for tyrosine hydroxylase in the amygdala nuclei, LA, the dorsal ITC (ITCd), CeA and the basal amygdala (BA), which are outlined with white dotted lines (left). A magnified view of the ITCd area within a solid red box clearly shows tyrosine hydroxylase-positive processes (right). Scale bars = 20 μm.

(B) Resting membrane potentials (RMPs) of the dorsal ITC neurons. DA was perfused during -5 - +5 min from application of STDP protocol for the induction of DA-LTD whereas PD-168077 was used for D4R-LTD. DA only group received no STDP protocol. RMPs were not significantly different between before and after any treatment (before DA-LTD, -85.48 ± 0.96 mV *vs.* after DA-LTD, -86.03 ± 0.66 mV; before D4R-LTD, -84.80 ± 0.72 mV *vs.* after D4R-LTD, -86.38 ± 0.65 mV; before DA, -84.97 ± 0.84 mV *vs.* after DA, -86.80 ± 0.81 mV; $p > 0.1$ for all, Wilcoxon test).

(C) Intrinsic membrane excitability that was measured by the number of action potentials (AP) elicited by current injection (left, 10-pA increment, 800 ms), was not different between before and after bath application of DA (N = 3, n = 7, $p > 0.05$ for all, Mann-Whitney U test for each injection current). Representative responses to a single injected current (60 pA) are shown before (right top) and after DA perfusion (right bottom).

(D) Perfusion of DA (30 μM, a green bar) did not affect synaptic transmission by itself (101.24 ± 8.54%, N = 5, n = 6, $p > 0.1$, Wilcoxon test). *Insert*: representative traces with color-matched time points.

(E) A representative time course of EPSPs upon DA-LTD induction. Duration of DA treatment is depicted with a green bar and the application of STDP protocol is denoted with a vertical black arrow.

(F) A summary histogram of STDP magnitude when various concentrations of DA were applied between -5 and +5 min from the application of STDP protocol (0 μM, 102.58 ± 9.75%, n = 4; 1 μM, 120.86 ± 5.83%, n = 5; 5 μM, 112.34 ± 5.63%, n = 4; 10 μM , 76.87 ± 3.09%, n = 5, ***$p < 0.001$; 30 μM, 68.56 ± 8.48%, n = 5, ***$p < 0.001$; 50 μM, 85.83 ± 5.98%, n = 6, **$p < 0.01$; 100 μM, 87.36 ± 11.03%, n = 4; 150 μM, 98.60 ± 6.16%, n = 5, Wilcoxon test relative

to the corresponding baselines).

(G) Representative images showing distribution of D4R in various nuclei of the amygdala. LA, ITCd, CeA and BA are delineated with white dotted lines. Those areas within white solid boxes in a low-magnification DAPI image (blue) were magnified for D4R immunostaining (red) with the merged DAPI staining for each area (right). Scale bars = 200 μm (left) and 10 μm (right).

(H) Number of D4R-immunoreactive puncta observed in the amygdala nuclei (LA, 7359.08 ± 587.07; BA, 13427.00 ± 1115.93; CeA, 14299.63 ± 1259.45; ITCd, 14648.40 ± 756.44, N = 3, n = 5-8).

(I) Representative images exhibiting partial co-localization of D4R and gephyrin. LA, ITCd and BA are delineated with white dotted lines (first from the left). Sequentially-magnified DAPI images (blue, first and second panels from the left) within white solid boxes were further analyzed with structured illumination microscope (SIM). SIM results revealed partial co-localization of D4R (green) and gephyrin (red). A merged image of D4R and gephyrin is represented with nuclei labelled with DAPI (far right). Scale bars = 500 μm (first from the left), 50 μm (second from the left) and 5 μm (right).

(J) Representative images exhibiting co-localization of D4R and synaptophysin. LA, ITCd and BA are delineated with white dotted lines (first from the left). Sequentially-magnified DAPI images (blue, first and second panels from the left) within white solid boxes were further analyzed with structured illumination microscope (SIM). SIM results revealed co-localization of D4R (green) and synaptophysin (red). A merged image of D4R and synaptophysin is represented with nuclei labelled with DAPI (far right). Scale bars = 500 μm (first from the left), 50 μm (second from the left) and 5 μm (right).

(K) Quantitative analysis for D4R co-localization with synaptic markers. 68.76 ± 3.24% of D4R-immunoreactive area was also positive for synaptophysin (N = 3, n = 12) while 45.07 ± 2.03% of D4R-immunoreactive area was also positive for gephyrin (N = 5, n = 11) (***$p < 0.001$, Mann-Whitney U test).

Data are represented as mean ± SEM.

Figure S4.

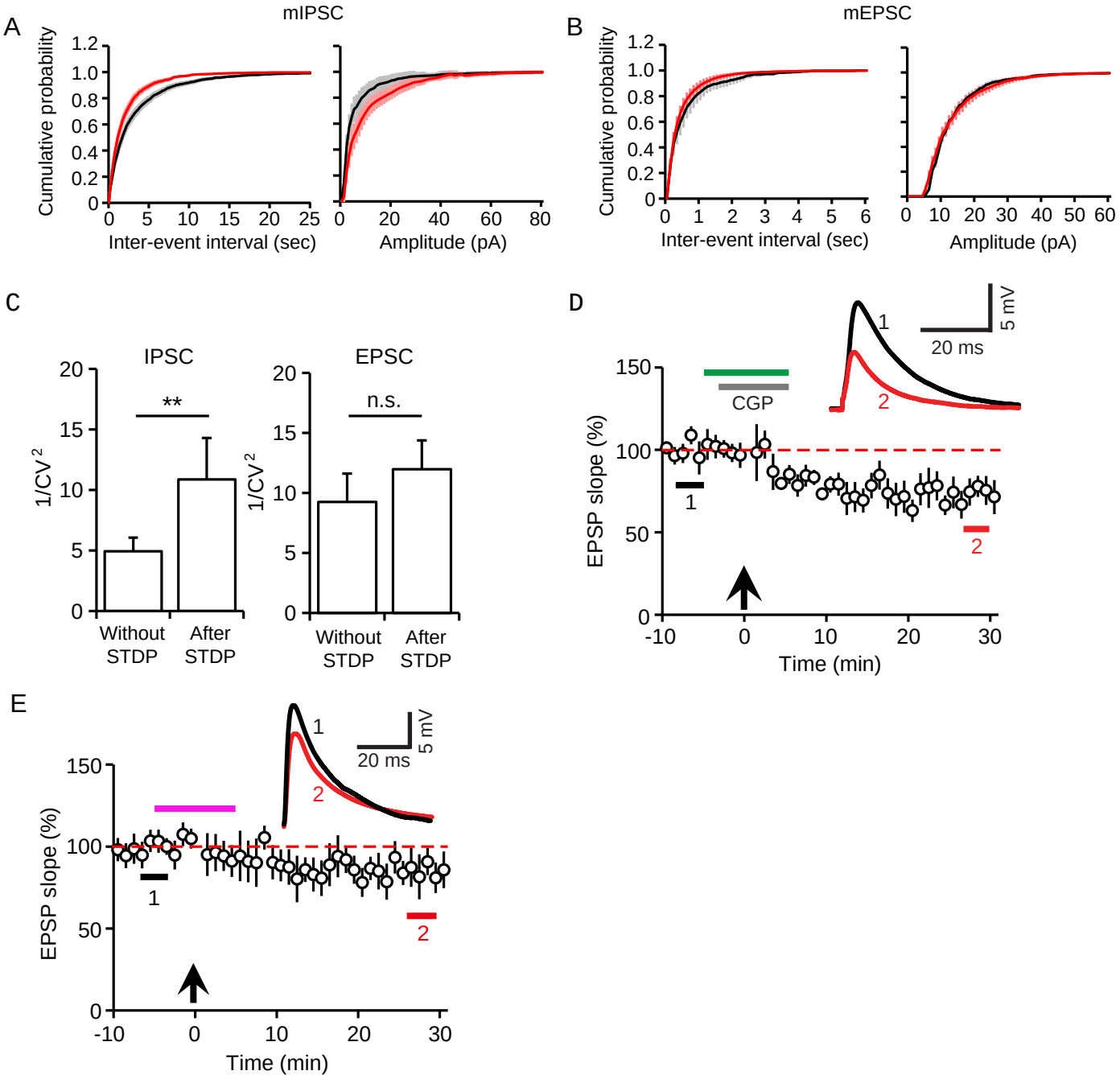
A
mIPSC
Cumulative probability
Inter-event interval (sec)
Amplitude (pA)
B
mEPSC
Cumulative probability
Inter-event interval (sec)
Amplitude (pA)
C
IPSC
**
EPSC
n.s.
1/CV2
Without STDP
After STDP
D
CGP
1
2
5 mV
20 ms
EPSP slope (%)
Time (min)
E
1
2
5 mV
20 ms
EPSP slope (%)
Time (min)

Figure S4, related to Figure 4.

(A) A cumulative probability plot of mIPSCs before (black) and after (red) DA-LTD induction (inter-event interval, $p < 0.001$; amplitude, $p < 0.01$; Kolmogorov-Smirnov test). Errors are indicated by shaded bars.

(B) A cumulative probability plot of mEPSCs before (black) and after (red) DA-LTD induction (inter-event interval, $p > 0.1$; amplitude, $p > 0.1$; Kolmogorov-Smirnov test). Errors are indicated by shaded bars.

(C) Quantal contents were estimated as $1/CV^2$ from either monosynaptic IPSCs or EPSCs elicited by minimal stimulation of the dorsal ITC or LA, respectively without or 10 min after the induction of DA-LTD ($1/CV^2$ for IPSCs: without STDP, 4.94 ± 1.12, N = 5, n = 13, after STDP, 10.87 ± 3.43, N = 4, n = 14, **p < 0.01, Mann-Whitney U test *vs.* $1/CV^2$ for EPSCs: without STDP, 9.25 ± 2.36, N = 6, n = 15; after STDP, 11.96 ± 2.42, N = 8, n = 19, $p > 0.1$, Mann-Whitney U test).

(D) CGP-46381 (10 μM, a gray bar), a $GABA_B$ receptor antagonist, was applied to examine a potential requirement of $GABA_B$ receptor activity for the induction of DA-LTD (73.16 ± 8.46%, N = 4, n = 5, $p < 0.05$, Wilcoxon test). Duration of DA treatment is depicted with a green bar and the application of STDP protocol is denoted with a vertical black arrow. *Insert*: representative traces are delineated with color-matched time points.

(E) Bath application of a D1R-antagonist, SCH-23390 (10 μM, a purple bar) rescued LTD after strong fear conditioning (-85.3 ± 10.9%, N = 3, n = 6, $p < 0.05$, Wilcoxon test). The application of STDP protocol is denoted with a vertical black arrow. *Insert*: representative traces with color-matched time points.

Data are represented as mean ± SEM.

Figure S5.

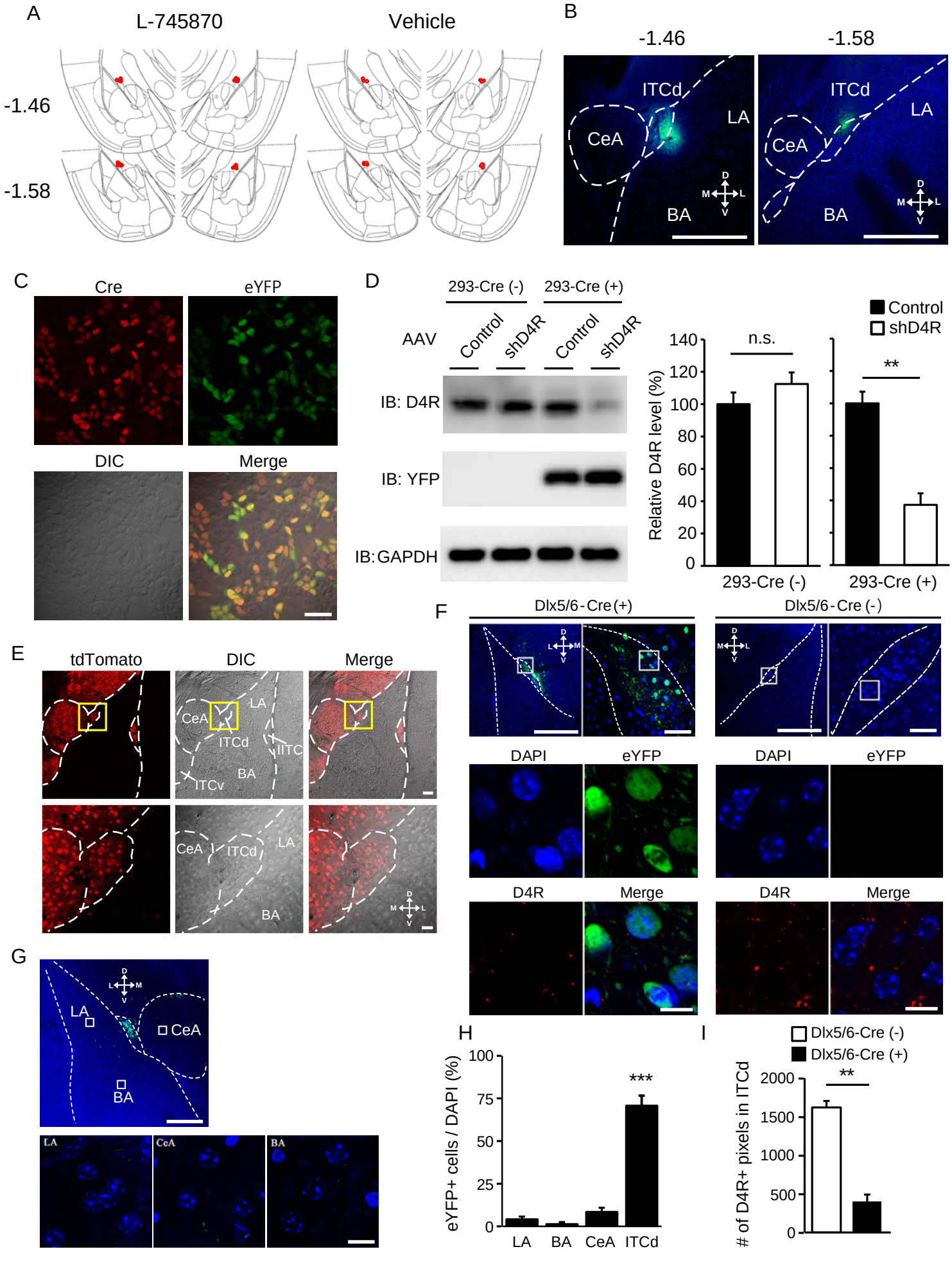
A
L-745870
Vehicle
-1.46
-1.58
B
-1.46
-1.58
ITCd
LA
CeA
BA
C
Cre
eYFP
DIC
Merge
D
293-Cre (-)
293-Cre (+)
AAV
Control
shD4R
Control
shD4R
IB: D4R
IB: YFP
IB: GAPDH
Control
shD4R
Relative D4R level (%)
n.s.
**
293-Cre (-)
293-Cre (+)
E
tdTomato
DIC
Merge
CeA
LA
ITCd
IITC
BA
ITCv
F
Dlx5/6-Cre (+)
Dlx5/6-Cre (-)
DAPI
eYFP
D4R
Merge
G
LA
CeA
BA
H
eYFP+ cells / DAPI (%)
***
LA
BA
CeA
ITCd
I
Dlx5/6-Cre (-)
Dlx5/6-Cre (+)
# of D4R+ pixels in ITCd
**

Figure S5, related to Figure 5.

(A) Histological reconstruction of drug infusion sites. Filled red circles indicate the locations of cannula tips in the images adapted from Franklin and Paxinos, 1997. Distances from the bregma (mm) are specified on the left sides.

(B) Merged fluorescence images of coronal sections obtained from two L-745870-injected mice. A mixture of L-745870 (500 nM) and FITC (green, 500 nM) was injected to the dorsal ITC areas. The diffusion range of L-745870 across the amygdala areas were estimated by that of FITC. Slices were counterstained with DAPI (blue) to delineate the amygdala nuclei, LA, the dorsal ITC (ITCd), CeA and the basal amygdala (BA) outlined with white dotted lines. Distances from the bregma (mm) are specified above images. Scale bars = 500 μm.

(C) Cre-mediated recombination of cKD-eYFP-shD4R leading to eYFP expression. The mixed culture of Cre (+) and Cre (-) HEK-293 cells was infected with rAAV2-cKD-eYFP-shD4R. After incubation, HEK-293 cells were immunostained for Cre (red, top left) and eYFP (green, top right). Fluorescence (top) and merged images (bottom right) along with the DIC image (bottom left) exhibit the selective expression of eYFP only in Cre (+) cells, but not in Cre (-) cells. Scale bar = 50 μm.

(D) Cre-mediated depletion of D4R. Either rAAV2-cKD-eYFP-shD4R or control rAAV2-cKD-eYFP was applied onto Cre (-) or Cre (+) HEK-293 cells which had been transfected with pCMV-D4R-turboGFP and then protein levels were analyzed from the cell lysates (left). D4R levels were markedly reduced by rAAV2-cKD-eYFP-shD4R only in Cre (+) HEK-293 cells, compared with those of control AAV without shD4R sequence or Cre (-) cells (middle, Cre (-): control, 100 ± 7.26%; shD4R, 112.5 ± 7.12%; $p > 0.1$, Mann-Whitney U test; right, Cre (+): control, 100 ± 8.20%; shD4R, 37.25 ± 4.09%; n = 5 for each group, $^{**}p < 0.01$, Mann-Whitney U test).

(E) A coronal section of the amygdala from Ai14 reporter mice mated with *Dlx5/6-Cre* (+) mice. tdTomato-positive neurons were observed mainly in striatum, CeA and ITCs including the dorsal, the ventral (ITCv) and the lateral ITC (lITC), but only scarcely in LA and BA (left). Individual nuclei of the amygdala are outlined with the anatomical features elucidated in the DIC image (middle). The merged image is also shown (right). The magnified views of the area within solid yellow boxes exhibit tdTomato expression in ITCd region (bottom). Scale bars =

100 μm (top) and 20 μm (bottom).

(F) *In vivo* validation of rAAV2-cKD-eYFP-shD4R. rAAV2-cKD-eYFP-shD4R was infused into ITCd areas of either *Dlx5/6-Cre* (+) (left) or *Dlx5/6-Cre* (-) mice (right). ITCd, external and intermediate capsules are delineated with white dotted lines in merged images of DAPI (blue) and eYFP (green)(top). Sequentially-magnified images exhibit the representative areas (top, white solid boxes), which were further magnified (bottom). The fluorescence and merged images show the distribution of D4R (red) around cell somas labelled with DAPI. Scale bars = 500 μm (top left), 50 μm (top right) and 10 μm (bottom).

(G) Representative fluorescence images of neighboring amygdala nuclei of a rAAV2-cKD-eYFP-shD4R-infused *Dlx5/6-Cre* (+) mouse. LA, CeA and BA are delineated with white dotted lines outlining external and intermediate capsules. Those amygdala areas within white solid boxes were magnified in the merged images of DAPI (blue) and eYFP (green) (bottom). No considerable expression of eYFP was observed in those areas (bottoms). Scale bars = 200 μm (top) and 10 μm (bottoms).

(H) Proportions of eYFP-positive cells in each amygdala nucleus normalized to the number of cells labelled by DAPI (LA, 3.98 ± 1.76%; BA, 1.19 ± 1.19%; CeA, 8.37 ± 2.54%; ITCd, 70.58 ± 6.05%; N = 5, ***$p < 0.001$, Kruskal–Wallis H test followed by Mann-Whitney U test).

(I) The number of pixels positive for D4R markedly decreased in ITCd of *Dlx5/6-Cre* (+) mice that received rAAV2-cKD-eYFP-shD4R compared with that of *Dlx5/6-Cre* (-) mice (*Dlx5/6-Cre* (+), 397.33 ± 94.51; *Dlx5/6-Cre* (-), 1621.00 ± 84.22; N = 5 for both groups, **$p < 0.01$, Mann-Whitney U test).

Data are represented as mean ± SEM.

Figure S6.

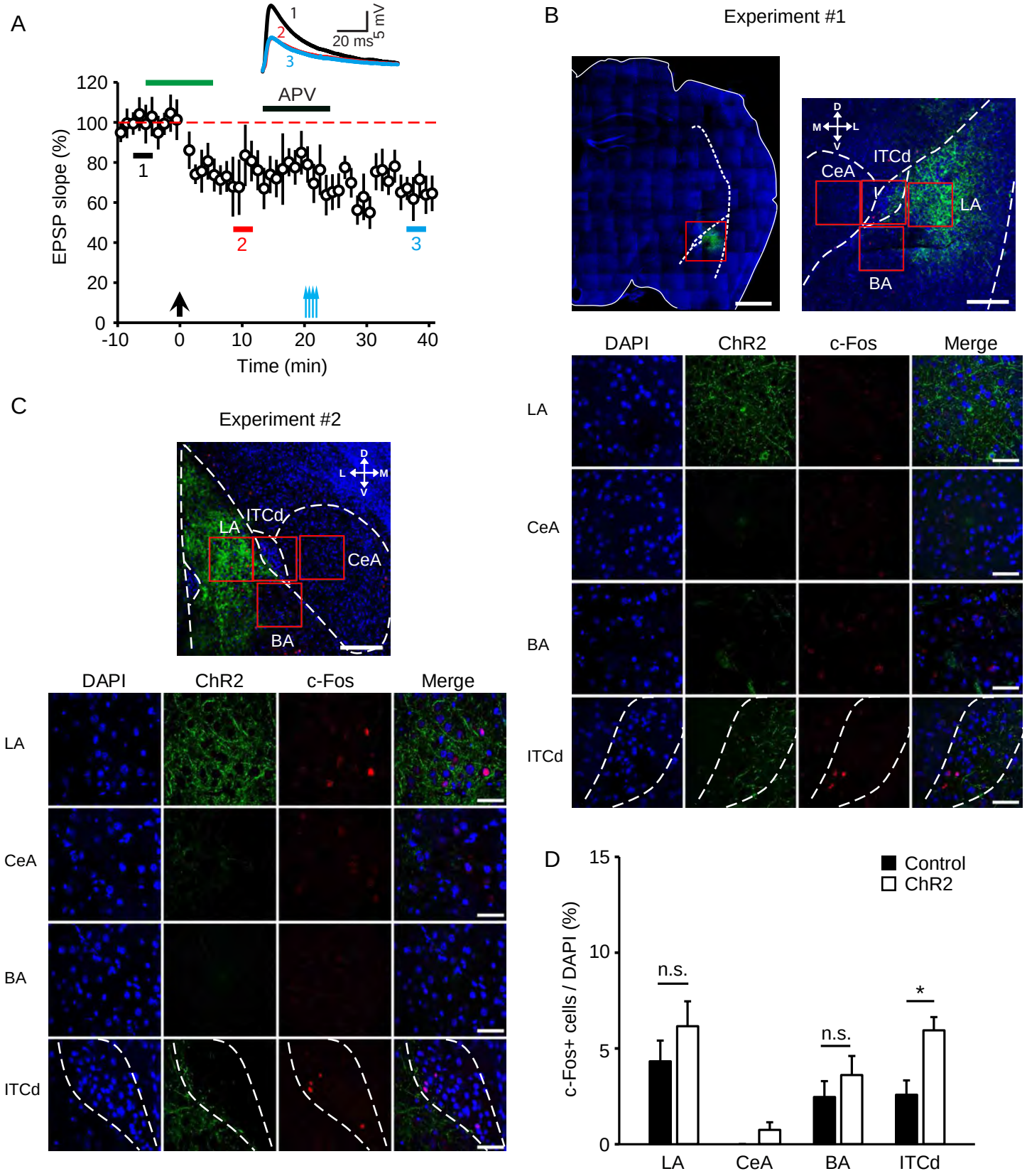
A
1
2
3
20 ms
5 mV
APV
EPSP slope (%)
Time (min)
B
Experiment #1
D
M
L
V
ITCd
CeA
LA
BA
DAPI
ChR2
c-Fos
Merge
C
Experiment #2
D
L
M
V
ITCd
LA
CeA
BA
DAPI
ChR2
c-Fos
Merge
LA
CeA
BA
ITCd
D
Control
ChR2
c-Fos+ cells / DAPI (%)
n.s.
n.s.
*
LA
CeA
BA
ITCd

Figure S6, related to Figure 6.

(A) Reversal of DA-LTD dependent upon NMDAR activity. TBS-like optic stimulation (vertical blue arrows) in the presence of APV (50 μM, a black bar) failed to restore EPSPs (65.76 ± 8.93%, N = 2, n = 5, $p < 0.05$, Wilcoxon test). Duration of DA treatment is depicted with a green bar and the application of STDP protocol is denoted with a vertical black arrow. *Inserts*: representative traces are delineated with color-matched time points.

(B) A single hemisphere from a mouse that had received rAAV5-CamKIIα-hChR2-eYFP (top left) is shown in the merged image of DAPI (blue) and eYFP (green). External/intermediate capsules and borderline of the brain slice are marked with white dotted lines and solid line, respectively. Areas containing the dorsal ITC (ITCd), LA, CeA or the basal amygdala (BA), are outlined with solid red boxes (top right) and further magnified (bottom). Magnified fluorescence and merged images indicate that c-Fos-positive cells (red) were readily observed in ITCd after *in vivo* optogenetic stimulation to the region centered around ITCd whereas ChR2 expression was most frequently observed in LA (bottom). However, c-Fos-positive cells were rarely detected in CeA and BA. Scale bars = 1 mm (top left), 200 μm (top right) and 20 μm (bottom).

(C) Another mouse that had received rAAV5-CamKIIα-hChR2-eYFP (top left) is shown in the merged image of DAPI (blue) and eYFP (green). Areas containing ITCd, LA, CeA or BA, are outlined with solid red boxes (top right) and further magnified (bottom). Magnified fluorescence and merged images indicate that c-Fos-positive cells (red) were readily observed in ITCd and LA presumably due to back-propagation of activity after *in vivo* optogenetic stimulation to the region centered around ITCd whereas ChR2 expression was mainly observed in LA (bottom). However, c-Fos-positive cells were rarely detected in CeA and BA. Scale bars = 1 mm (top left), 200 μm (top right) and 20 μm (bottom). Scale bars = 200 μm (top) and 20 μm (bottom).

(D) *In vivo* optical stimulation significantly increased proportions of c-Fos-positive cells normalized to the number of cells labelled by DAPI when rAAV5-CamKIIα-hChR2-eYFP was infused into LA (LA: control, 4.33 ± 1.08% *vs*. ChR2, 7.46 ± 1.52%; CeA: control, 0.00 ± 0.00 *vs*. ChR2, 0.98 ± 0.53%; BA: control, 2.46 ± 0.83% *vs*. ChR2, 4.35 ± 1.15%; ITCd: control, 2.58 ± 0.75% *vs*. ChR2, 5.91 ± 0.86%; N = 6, *$p < 0.05$, Mann-Whitney U test).

Data are represented as mean ± SEM.

Figure S7.

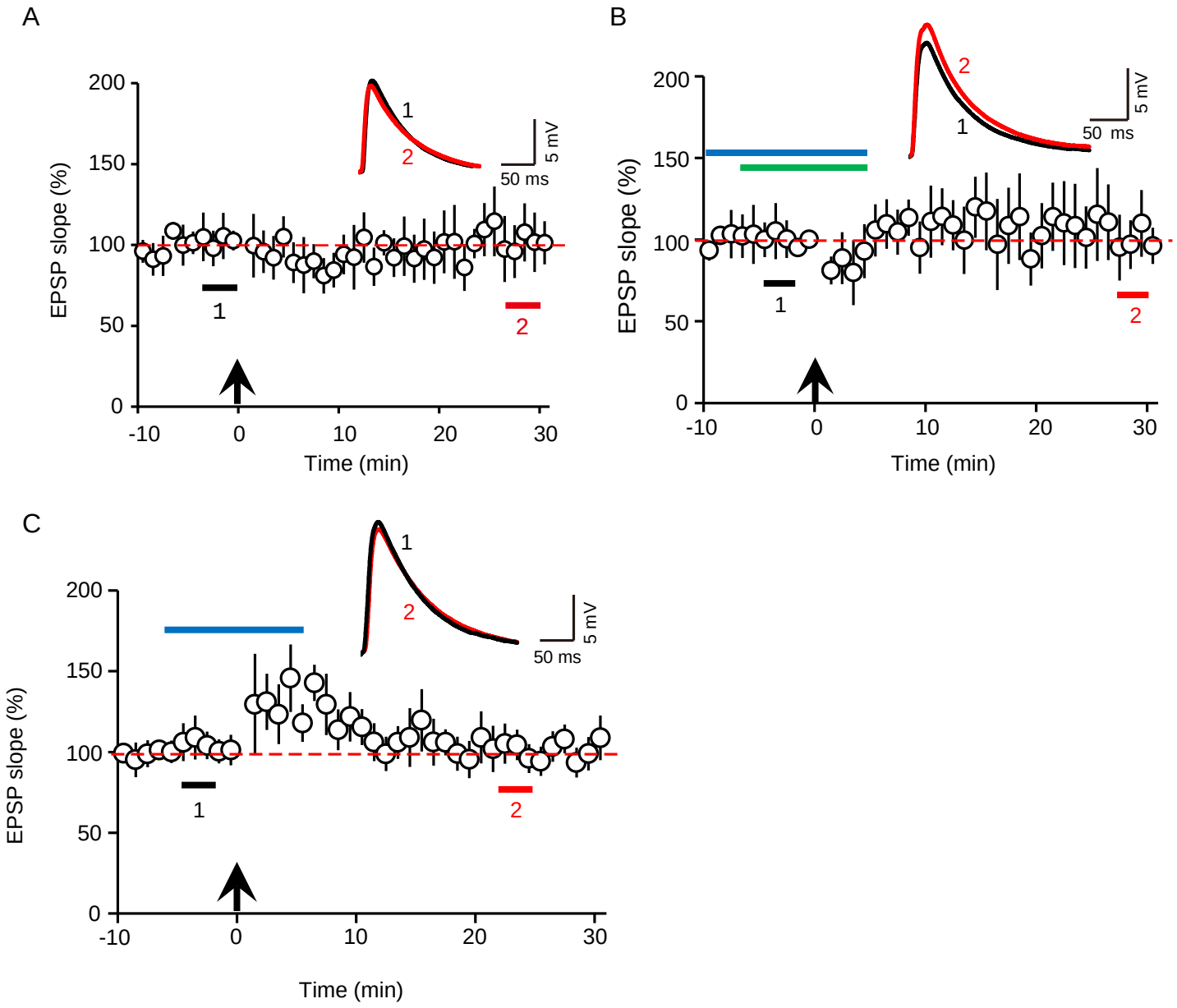

Figure S7, related to Figure 7.

(A) STDP was assessed 24 hours after CORT injection (5 mg/kg, i.p.) without weak fear conditioning. No synaptic plasticity arose in the LA-dorsal ITC pathway (101.68 ± 17.08%, N = 4, n = 5, $p > 0.1$, Wilcoxon test). *Insert*: representative traces with color-matched time points. The application of STDP protocol is denoted with a vertical black arrow.

(B) DA-LTD was abolished by perfusion of a CORT antagonist, RU38486 (1 μM, a blue bar) (105.81 ± 20.95%, N = 3, n = 5, $p > 0.1$, Wilcoxon test). *Insert*: representative traces with color-matched time points. Duration of DA treatment is depicted with a green bar and the application of STDP protocol is denoted with a vertical black arrow.

(C) Perfusion of RU38486 (1 μM, a blue bar) prevented LTD from being induced after weak fear conditioning (101.46 ± 10.59%, N = 3, n = 5, $p > 0.1$, Wilcoxon test). *Insert*: representative traces with color-matched time points. The application of STDP protocol is denoted with a vertical black arrow.

Data are represented as mean ± SEM.

Table S1.

Parameter	Average	SEM	n (N)
RMP (mV)	-85.3	2.5	15 (5)
Rin (MΩ)	650	65.4	12 (7)
Cm (pF)	61	4.2	14 (6)
AHP (mV)	-9	0.51	9 (5)
Amplitude of AP (mV)	69	3.5	10 (10)
Half-width of AP (ms)	0.76	0.04	9 (8)

Table S1, related to Figure 1. Electrophysiological properties of the dorsal ITC neurons.

RMP, resting membrane potential; Rin, input resistance; Cm, membrane capacitance; AHP, afterhyperpolarization; AP, action potential.

Supplemental Experimental Procedures

Animals

Male C57BL/6J, D4R-KO, and *Dlx5/6-Cre* and Ai14 reporter mice from Jackson Laboratory (Bar Harbor, ME) were housed under a 12-hour light/dark cycle and given *ad libitum* access to food and water. All procedures for animal experiments were approved by the ethical review committee of POSTECH (Pohang University of Science & Technology), Korea and performed in accordance with the relevant guidelines.

Plasmid and viral vectors

pCMV6-AC-D4R-turboGFP was purchased from OriGene Technologies (Rockville, MD). shRNA sequences targeting D4R (gctgctcatcggcttggtgtt) were also obtained from OriGene Technologies and cloned into pLL3.7 construct (Rubinson et al., 2003). Then, the effectiveness of shD4R sequence was verified with quantitative RT-PCR using HEK-293 cells (GenTarget, San Diego, CA) co-transfected with pCMV6-AC-D4R-turboGFP and pLL3.7-shD4R. To achieve simultaneous Cre-dependent knock-down and eYFP expression in the same cells, pAAV-EF1a-DIO-eYFP obtained from K. Deisseroth, was modified by inserting U6 promoter and TATAlox and adding new sequences (Supplemental Text). The resultant plasmids, cKD-eYFP-shD4R (pAAV-EF1α-DIO-TATAlox-eYFP-U6-shD4R) and control cKD-eYFP (pAAV-EF1α-DIO-TATAlox-eYFP-U6) vectors were used for production of the corresponding viruses.

Virus production was conducted in accordance to established protocols (Hommel et al., 2003). Briefly, HEK-293 cells were co-transfected with helper plasmids and either cKD-eYFP-shD4R or cKD-eYFP at an equal molar ratio using Lipofector-Q transfection reagents (AptaBio, Korea). 72 hours after co-transfection, the cells were lysed through freeze-thaw steps and resultant AAV particles were purified by iodixanol-gradient ultracentrifugation at 340,000 *g* for 2 hours. AAV particles were concentrated with Amicon Filter (100K, Millipore, Bedford, MA) to achieve at least 5.0×10^{12} gc/ml.

Western blot

Normal HEK-293 and Cre-expressing HEK-293 were cultured in Dulbecco's modified Eagle's

medium (DMEM) supplemented with 10% fetal bovine serum (Hyclone, South Logan, UT) and 100 U/ml penicillin and 100 g/ml streptomycin. They were incubated at 37°C/5% CO_2. For heterologous expression of D4R, we transfected HEK-293 cells with pCMV-D4R-turboGFP using Lipofector-Q. D4R-transfected cells were further treated with either rAAV2-cKD-eYFP or rAAV2-cKD-eYFP-shD4R. 2 days after viral infection, total proteins were extracted using HEPES lysis buffer (40 μM HEPES, 120 mM NaCl, 1 mM EDTA, 1% Triton X-100) containing protease inhibitor cocktail (Roche, Indianapolis, IN), separated on 10% SDS PAGE gel and then transferred onto PVDF membrane (0.45 μm pore, Millipore). The membranes were blocked for 1 hour in TBST (Tris-buffered-saline and Tween 20) containing 5% skim milk and then individually incubated overnight at 4°C with anti-D4R (sc-31481, 1:1000, Santa Cruz, Paso Robles, CA), anti-GFP (LF-PA0043, 1:1000, AbFrontier, Korea) or anti-GAPDH (sc-25778, 1:1000, Santa Cruz) antibodies. HRP-conjugated anti-goat (sc-2020, 1:5000, Santa Cruz) or anti-rabbit (A120-201P, 1:5000, Bethyl Laboratories, Montagomery, TX) antibodies were applied as secondary antibodies and treated at room temperature (RT) for 1 hour. Western blots were visualized with ECL reagent (WBKLS0100, Millipore) and scanned with LAS-4000 (GE Heath Care, Piscataway, NJ). Quantitative analysis was performed with ImageJ (NIH, Bethesda, MD).

Immunocytochemistry

HEK-293 cells were plated onto 12-mm glass coverslips coated with 0.1 mg/ml poly-L-lysine and then treated with either rAAV2-cKD-eYFP-shD4R or rAAV2-cKD-eYFP. Following 3 days-incubation, the coverslips were fixed with a fixative solution containing 4% paraformaldehyde in phosphate buffered saline (PBS) at 4°C for 24 hours and permeabilized with 0.25% Triton X-100 in PBS at 25°C for 10 minutes. Then the samples were blocked with 1% BSA, 5% normal goat serum and 0.25% Triton X-100 in PBS. For Cre staining, anti-Cre (MAB3120, 1:500, Millipore) antibody was applied at 4°C for 12 hours and then goat anti-mouse Alexa Fluor 568 conjugated IgG (A11004, 1:500, Invitrogen, Carlsbad, CA) antibody at RT for 1 hour. The samples were mounted on glass slides with mounting medium (Santa Cruz) containing DAPI.

Immunohistochemistry

Mice were deeply anesthetized with tribromoethanol (250 mg/kg) and transcardially perfused with PBS and then a fixative solution (4% paraformaldehyde in PBS). The isolated brains were kept in the fixative solution for overnight at 4°C. The brains were embedded in 5% agarose and sliced into 50-μm thick coronal sections with a vibratome (VT1000S, Leica, Germany). Sliced sections were blocked with 4% normal donkey serum and 0.4% Triton X-100 in PBS at 4°C for 1 hour and then were incubated with goat anti-D4R (sc-31481; 1:500, Santa Cruz), rabbit anti-synaptophysin (04-1019; 1:1000, Millipore) or mouse anti-gephyrin (sc-25311, 1:300, Santa Cruz) antibodies at 4°C overnight. Donkey anti-goat DyLight 488 conjugated IgG (1:300, Bethyl Laboratories) or donkey anti-goat Alexa Fluor 594 conjugated IgG (1:300, Invitrogen), donkey anti-rabbit Alexa Fluor 568 conjugated IgG (1:300, Invitrogen) or DyLight 550 conjugated donkey anti-mouse IgG (1:300, Bethyl Laboratories) antibodies were used as secondary antibodies. For c-Fos staining, we used rabbit anti-c-Fos (sc-52, 1:500, Santa Cruz) as primary antibody and goat anti-rabbit Alexa Fluor 647 conjugated IgG (1:500, Invitrogen) as secondary antibody after blocking with 4% normal goat serum in PBS. All tissues were mounted on the slide glasses with UltraCruz mounting medium (Santa Cruz).

Cellular imaging

We used laser scanning confocal microscopes (LSM 510, Zeiss, Germany or Fluoview 1000, Olympus, Japan) for cellular imaging experiments except for co-localization between D4R and synaptic marker proteins. We also used a structured illumination microscope (N-SIM, Nikon, Japan) to examine co-localization of D4R and gephyrin/synaptophysin further precisely rather than conventional confocal microscopy. Quantitative analysis of immunoreactive puncta was performed using MetaMorph 7.7 software (Molecular Devices, Sunnyvale, CA).

Post-embedding immuno-gold electron microscopy

Immuno-EM was conducted in accordance with established protocols (Masugi-Tokita and Shigemoto, 2007). Transcardial perfusion and preparation of brain slices were identical to those used for the immunohistochemistry experiments except thickness of slices being 200 μm. The dorsal ITC areas were isolated from the amygdala slices under a dissection microscope (Olympus). The tissue was immersed into a 0.001% osmium tetroxide (OsO_4) solution on the ice for 1 hour to achieve the membrane preservation and then rinsed with PBS. Then, the tissue

was kept in a 10% sucrose solution for cryoprotection. High-pressure freezing system (HPM 100, Leica) was used to acutely freeze the tissue while preserving the membrane and cellular components. After acute freezing, sample tissue was kept in acetone and embedded in Lowicryl HM20 resin (Electron microscopy sciences, Hatfield, PA) at -45°C for 2 days and UV-polymerization for 1 day with EM AFS2 (Leica). UV-polymerized blocks containing the dorsal ITC tissues were sliced by an ultra-microtome (Leica). These slices were then put on the Nickel grids (FCF200-Ni, Electron microscopy sciences). For immunostaining, goat anti-D4R (1:20, Millipore) and mouse monoclonal anti-GAD67 (MAB5406, 1:20, Millipore) antibodies were used as primary antibodies. Subsequently, 12-nm gold particle-Donkey anti-goat or 6-nm gold particle-Donkey anti-mouse (705-205-147 and 715-195-150, respectively, Jackson Immuno Research, West Grove, PA) antibodies were used for labeling D4R or GAD-67, respectively after blocking with 0.2% normal donkey serum in detergent-free PBS at 4°C overnight. After antibody application, we treated 1 - 2% uranyl acetate for 4 minutes and Reynolds solution for 2 minutes to obtain a high-contrast image. Images were obtained with a transmission electron microscope (JEM-1011, Jeol, Japan).

Virus infusion and implantation of tungsten electrodes and optic fibers

After mice were anesthetized with ketamine and xylazine, the head was fixed in a stereotaxic frame (Kopf, Tujunga, CA). For viral infusion, ~0.1 µl of virus solution was infused using horizontally pulled glass needles, into each hemisphere with NanojectII (Drummond scientific instrument, Broomall, PA) for 1 minute (4 injections per hemisphere were applied, 23.0 nl per injection which had a rate of 46 nl/sec), and the injection needles remained for additional 10 minutes to allow diffusion of AAV. Coordinates were as follows for infusion to the lateral nucleus (LA) of the amygdala: AP -1.4 mm, ML ±3.4 mm, DV -4.0 mm from the bregma, for infusion to the infralimbic region (IL) of the medial prefrontal cortex (mPFC): AP +1.9 mm, ML ±0.3 mm, DV -2.5 mm from the bregma, for infusion to the prelimbic region (PL) of mPFC: AP +1.9 mm, ML ±0.3 mm, DV -1.5 mm from the bregma, and for infusion to the dorsal ITC: AP -1.4 mm, ML ±3.2 mm, DV -4.2 mm from the bregma. Single tungsten electrodes were ipsilaterally implanted to reach the dorsal ITC for recording *in vivo* activity and IL for *in vivo* stimulation in the aforementioned coordinates, and secured with screws and dental cement. To ensure the recording electrodes were placed correctly in the dorsal ITC, we electrically stimulated IL (0.1 Hz) while neural activity was monitored from the dorsal ITC. If burst-like

spikes were observed earlier than 50 ms from each IL stimulation, the recording electrodes were secured with dental cement. Optic fibers (50-μm core diameter, ThorLabs, Newton, NJ) were secured to a multi-mode zirconia ceramic ferrule (Precision Fiber Products, Milpitas, CA) with adhesive and epoxy, and then implanted to place its tip on the dorsal atop of the dorsal ITC in the coordinate, AP -1.4 mm, ML ±3.2 mm, DV -4.0 mm from the bregma, and secured with dental cement.

Drug infusion

Guide cannulae were implanted bilaterally (26 gauge, Plastics One, Roanoke, VA) aimed into the dorsal ITC areas in the coordinates, AP -1.4 mm, ML ±3.2 mm, DV -4.2 mm from the bregma, and were fixed in the skull with dental cement. The cannulae remained capped with internal dummy cannulae (33 gauges, Plastics One) after surgery. Animals were individually housed and allowed to recover at least for 1 week after surgery. The mice bilaterally received 0.5 μl of either L-745870 or vehicle through the injection cannula (33 gauge, Plastics One) connected to a 10-μl Hamilton syringe for 5 minutes at a rate of 0.1 μl/min using microinfusion pump (Harvard Apparatus, Holliston, MA) 20 minutes before fear conditioning. L-745870 was dissolved to 500 nM in 0.9% saline just before the infusion. Mice were kept with injector cannulae for additional 5 minutes after the end of infusion and then were subjected to fear conditioning. To estimate the diffusion range of L-745870, FITC (500 nM) was also included in the injectant for certain experiments. The subject mice were transcardially perfused right after the last behavioral tests and analyzed for the injection loci. Data from the animals with wrong placement of cannula tips were excluded from further analyses.

Behavioral tests

We used two different chambers (26 cm x 26cm x 24 cm). Context A consisted of black opaque PVC walls and a grid floor, which was swiped with 70% ethanol before each trial whereas context B consisted of transparent plastic walls and a PVC floor covered with cage bedding and was scented with peppermint odor. Fear conditioning trainings were conducted in context A within sound-attenuating conditions (Panlab, Spain). Tone CS (conditioned stimulus) was delivered with a speaker while electric foot shock US (unconditioned stimulus) was applied through a floor grid attached to a shock generator (Panlab). The chambers were also equipped with infrared webcams connected to a personal computer to store animal behavior. Mice were

placed in the context A for 2 minutes of acclimation and were then presented with auditory tone (CS: 3 kHz, 80 dB for 30 sec) that were co-terminated with electric foot shocks (US: 0.4 or 0.8 mA for 0.5 sec). Total 8 CS-US pairs were presented in pseudorandom intertrial intervals (varied from 60 to 120 sec). 24 hours after fear conditioning, mice were placed in context B to assess the recall of fear memory by being re-exposed to CS, but without US for 2 minutes. For the tone-only control group, fear conditioning and fear recall were performed without presentation of US. For the unpaired conditioning group, CS and US (0.8 mA for 0.5 sec) were separately presented with pseudorandom interval (varied from 60 to 120 sec). Freezing behavior was measured as the time duration of absence in all movements except respiration.

In order to reverse LTD-like plasticity, optogenetic TBS was applied onto the dorsal ITC areas through the optic fibers. 1 day after 20-min habituation to context A, the optic fiber-implanted mice were fear conditioned in context A with sub-threshold US (0.4 mA). At the next day freezing levels of those mice were tested with 2 separate recall sessions, each of which was composed of 2-min presentation of CS in the context B. Optogenetic TBS was delivered at the home cage, 30 minutes after the first recall session. 30 minutes after application of optogenetic TBS, fear recall was tested again in the same context used for the first recall test.

To induce PTSD-like memory impairment, corticosterone (CORT, 5 mg/kg) or vehicle was intraperitoneally (i.p.) injected immediately after fear conditioning as previously described (Kaouane et al., 2012). The cue-conditioning group underwent weak fear conditioning with the previously-described CS-US pairing paradigm in context A and was tested for fear recall toward the cue in context B at the next day. To assess contextual fear memory from cue-conditioned animals, the mice were placed again in context A 2 hours after termination of the first recall test and then duration of freezing was measured for 2 minutes without presentation of the auditory cue. The context-conditioning group received two sets of unpaired shocks and tones (electric shocks and tones with 20 sec interval) in context A and was tested for fear recall in context A at the next day. To assess auditory fear memory from context-conditioned animals, the mice were placed in context B 2 hours after termination of the first recall test and the freezing time during presentation of the auditory cue was measured for 2 minutes.

ChR2-mediated optical stimulation

rAAV5-CamKIIα-hChR2(H134R)-eYFP and rAAV5-CamKIIα-eYFP from Vector Core of

University of North Carolina were used for optogenetic manipulation. Optical activation of axon terminals of the dorsal ITC neurons for STDP induction was performed by illuminating acute slices with 1-msec blue light pulses from LED source (ThorLabs). The light intensity was adjusted to evoke robust EPSPs (~70% success rate, Kyuyoung and Huguenard, 2014). 473-nm DPSS blue laser (Shanghai Laser & Optics Century, China) was utilized to apply *in vivo* optogenetic TBS to the LA-dorsal ITC pathway. The optogenetic TBS was delivered through a custom-made patch cable (50-μm core diameter fiber optics, ThorLabs). This TBS was composed of 10 sets of light pulses at 0.1 Hz, each set of 10 pulse trains at 5 Hz, and a single train had 4 light pulses at 50 Hz. The generation of optogenetic TBS was controlled by Master-8 stimulator (AMPI, Israel). During optogenetic TBS, the mice were allowed to freely move nearby their home cage without any anesthetization (Pascoli et al., 2012). The intensity of blue laser was calibrated using powermeter (ThorLabs) to ~0.5 mW/mm^2 at 150 μm below the tip of the optic fiber (Witten et al., 2011). The putative light loss was carefully compensated for attenuation through the implanted part, which was measured prior to the surgery. Geometric light loss in the brain was also predicted and compensated with the web-based light transmission calculator (http://optogenetic.org/). After transcardial perfusion, we validated that each optic fiber withdrawn from the skull did not exhibit a significant difference in light loss from the measurement prior to the surgery (Sparta et al., 2012).

Slice electrophysiology

Acute brain slices were placed in recording chambers and continuously superfused (2 ml/min) with a bathing solution containing 119 mM NaCl, 2.5 mM KCl, 2.5 mM $CaCl_2$, 2 mM $MgSO_4$, 1.25 mM NaH_2PO_4, 26 mM $NaHCO_3$, and 10 mM D-glucose while equilibrated with 95% O_2 and 5% CO_2 (pH 7.3 - 7.4) at RT. Whole-cell patch recordings in current clamp mode or voltage clamp mode were made with a MultiClamp 700B amplifier (Molecular Devices). Recording electrodes (8-10 MΩ) were filled with an internal solution containing, for EPSP recordings: 120 mM K-gluconate, 5 mM NaCl, 1 mM $MgCl_2$, 0.2 mM EGTA, 10 mM HEPES, 2 mM MgATP, and 0.1 mM NaGTP at pH 7.2 adjusted with KOH, for EPSC recordings: 130 mM $CsMeSO_4$, 8 mM NaCl, 0.5 mM EGTA, 10 mM HEPES, 2 mM MgATP, 0.1 mM NaGTP, 5 mM QX-314, 10 mM phosphocreatine at pH 7.2 adjusted with CsOH (Kwon et al., 2008), for IPSP recordings: 135 mM KCl, 10 mM NaCl, 2mM $MgCl_2$, 0.5 mM EGTA, 10 mM HEPES, 2 mM MgATP, 0.1 mM NaGTP at pH 7.2 adjusted with KOH (Roberto et al., 2003), and for IPSC recordings: 135 mM CsCl, 1 mM EGTA, 10 mM HEPES, 2 mM MgATP, 0.1 mM NaGTP,

and 5 mM QX-314 at pH 7.2 adjusted with CsOH (Maximov et al., 2007). Exceptionally, to compare mPSCs without or after STDP, KCl-based and K-gluconate-based internal solutions were used for recording mIPSCs and mEPSCs, respectively. K-gluconate based solution was also used to record EPSCs and IPSCs evoked by interleaved stimulation. Series resistance (10-30 MΩ) was monitored throughout all experiments. mEPSCs were recorded at -70 mV holding potential in the presence of 1 μM tetrodotoxin (TTX) and 100 μM picrotoxin (Tocris, UK) while mIPSCs were measured at -70 mV in the presence of 1 μM TTX, 25 μM NBQX, and 50 μM 2-amino-5-phosphonovaleric acid (APV, Tocris). Miniature PSCs were analyzed with MiniAnalysis (Synaptosoft, Fort Lee, NJ) or Clampfit 10.1 software (Molecular Devices). For PSC recordings with interleaved stimulation, the holding potential was briefly (~40 ms) changed from -70 mV to +10 mV to reach the reversal potential of EPSC for isolation of putative IPSCs. For STDP experiments, stimulus intensity was adjusted to elicit EPSPs displaying 25% - 30% of the maximum amplitudes. After obtaining stable baseline recording, 80 presynaptic stimuli were delivered at 2 Hz via metal stimulating electrode placed in LA while paired with action potentials induced by injection of depolarizing current to postsynaptic neurons (Shin et al., 2006). Quantal contents were estimated by obtaining the inverse square of the coefficient of variation ($1/CV^2$). Each $1/CV^2$ value was measured and calculated from 50 EPSCs or 50 IPSCs (80 % success rate for both PSCs), as previously described (Malinow and Tsien, 1990; Hodgkiss and Kelly, 2001).

GDPβS (0.5 mM) was included in the internal solution to examine the presynaptic/postsynaptic contribution of D4R-mediated signaling to DA-LTD. Liquid junction potential between K-gluconate based internal solution and extracellular ACSF (13.3 mV) was corrected for the representation of resting membrane potential (Figure S3B and Table S1). For a subset of neurons, neurobiotin (0.5%, Vector Labs, CA) was included in pipette solution for morphological characterization. There was no significant difference between the electrophysiological data from the neurons recorded with or without neurobiotin, and thus those data were combined. The neurobiotin-injected neurons were visualized by staining with Texas Red conjugated avidin (Vector Labs) after overnight fixation.

In vivo electrophysiology

Electrode-implanted mice were weakly anesthetized with ketamine and xylazine for the stable recording of spontaneous firings of the dorsal ITC neurons. Spontaneous firings were recorded

1 hour after the habituation session (before fear conditioning). Weak fear conditioning was conducted at 24 hours after the first *in vivo* recording. 24 hours after fear conditioning, spontaneous firings were recorded in the same manner (after fear conditioning). Signals from recording electrodes were amplified 10^4 times and band-pass filtered between 10 kHz (low-pass) and 300 Hz (high-pass) with DAM80 differential amplifier (World Precision Instruments, Sarasota, FL), and digitized at 40 kHz using PowerLab/4sp (ADinstruments, Colorado Springs, CO). Spontaneous firings were further processed and monitored with Chart acquisition software (ADinstruments). Single units were sorted using Spike2 software (Cambridge Electronic Design, UK), as previously described (Kim et al., 2014). A single spike was initially detected by an amplitude threshold. All detected spike traces were isolated by comparing with template waveforms. If not matched with any existing templates, a new template waveform was created based on the waveform of the detected spike. The spike isolation was refined by principle component analysis. Units showing inter-spike interval less than 1 ms were discarded from further analysis. Total spike numbers from each unit were used to calculate the spontaneous firing frequency of the dorsal ITC neuron. The electrode placements were thoroughly ascertained via post mortem examination.

Statistics

For multiple comparisons, non-parametric Kruskal-Wallis H test followed by Mann-Whitney U test with Bonferroni correction was utilized except for disynaptic IPSP measurement where repeated measures ANOVA and post hoc Bonferroni test were used (Figure 4C). For pairwise tests including assessment of synaptic plasticity, we took advantage of Wilcoxon signed-rank test. For assessment of synaptic plasticity, PSPs from 20-30 min after induction were compared to their own baseline. Mann-Whitney U test was used to compare two unpaired groups. Kolmogorov-Smirnov test was utilized for the cumulative distribution of miniature PSCs. Pearson's correlation coefficient was calculated to examine significance of a linear correlation. The number of animals and experiments are specified with N and n, respectively. All values indicated are means ± SEM and the statistical significance is presented with n.s. (non-significant) or asterisks, p values of < 0.05 (*), < 0.01 (**), and < 0.001 (***).

Supplemental References

Atasoy, D., Aponte, Y., Su, H.H., and Sternson, S.M. (2008). A FLEX switch targets Channelrhodopsin-2 to multiple cell types for imaging and long-range circuit mapping. J. Neurosci. *28*, 7025–7030.

Franklin, K., and Paxinos, G. (1997). The Mouse Brain in Stereotaxic Coordinates (San Diego: Academic Press)

Hodgkiss, J.P., and Kelly, J.S. (2001). Effect of FK960, a putative cognitive enhancer, on synaptic transmission in CA1 neurons of rat hippocampus. J. Pharmacol. Exp. Ther. *297*, 620–628.

Kasim, V., Miyagishi, M., and Taira, K. (2004). Control of siRNA expression using the Cre-loxP recombination system. Nucleic Acids Res. *32*, e66.

Kim, J., Kwon, J.-T., Kim, H.-S., Josselyn, S.A., and Han, J.-H. (2014). Memory recall and modifications by activating neurons with elevated CREB. Nat. Neurosci. *17*, 65-72.

Kyuyoung, C.L., and Huguenard, J.R. (2014). Modulation of short-term plasticity in the corticothalamic circuit by group III metabotropic glutamate receptors. J. Neurosci. *34*, 675–687.

Maximov, A., Shin, O.-H., Liu, X., and Südhof, T.C. (2007). Synaptotagmin-12, a synaptic vesicle phosphoprotein that modulates spontaneous neurotransmitter release. J. Cell Biol. *176*, 113–124.

Pascoli, V., Turiault, M., and Lüscher, C. (2012). Reversal of cocaine-evoked synaptic potentiation resets drug-induced adaptive behaviour. Nature *481*, 71–75.

Le Pichon, C.E., and Chesler, A.T. (2014). The functional and anatomical dissection of somatosensory subpopulations using mouse genetics. Front. Neuroanat. *8*, 1–18.

Lee, S., Yoon, B.-E., Berglund, K., Oh, S.-J., Park, H., Shin, H.-S., Augustine, G.J., and Lee, C.J. (2010). Channel-mediated tonic GABA release from glia. Science *330*, 790–796.

Masugi-Tokita, M., and Shigemoto, R. (2007). High-resolution quantitative visualization of glutamate and GABA receptors at central synapses. Curr. Opin. Neurobiol. *17*, 387–393.

Roberto, M., Madamba, S.G., Moore, S.D., Tallent, M.K., and Siggins, G.R. (2003). Ethanol increases GABAergic transmission at both pre- and postsynaptic sites in rat central amygdala neurons. Proc. Natl. Acad. Sci. U. S. A. *100*, 2053–2058.

Rubinson, D.A., Dillon, C.P., Kwiatkowski, A.V., Sievers, C., Yang, L., Kopinja, J., Rooney, D.L., Zhang, M., Ihrig, M.M., McManus, M.T., et al. (2003). A lentivirus-based system to functionally silence genes in primary mammalian cells, stem cells and transgenic mice by RNA interference. Nat. Genet. *33*, 401–406.

Sohal, V.S., Zhang, F., Yizhar, O., and Deisseroth, K. (2009). Parvalbumin neurons and gamma rhythms enhance cortical circuit performance. Nature *459*, 698–702.

Sparta, D.R., Stamatakis, A.M., Phillips, J.L., Hovelsø, N., van Zessen, R., and Stuber, G.D. (2012). Construction of implantable optical fibers for long-term optogenetic manipulation of neural circuits. Nat. Protoc. *7*, 12–23.

Ting, J.T., and Feng, G. (2014). Recombineering strategies for developing next generation BAC transgenic tools for optogenetics and beyond. Front. Behav. Neurosci. *8*, 1–13.

Tiscornia, G., Tergaonkar, V., Galimi, F., and Verma, I.M. (2004). CRE recombinase-inducible RNA interference mediated by lentiviral vectors. Proc. Natl. Acad. Sci. U. S. A. *101*, 7347–7351.

Ventura, A., Meissner, A., Dillon, C.P., McManus, M., Sharp, P., Van Parijs, L., Jaenisch, R., and Jacks, T. (2004). Cre-lox-regulated conditional RNA interference from transgenes. Proc. Natl. Acad. Sci. U. S. A. *101*, 10380–10385.

Witten, I.B., Steinberg, E.E., Lee, S.Y., Davidson, T.J., Zalocusky, K.A., Brodsky, M., Yizhar, O., Cho, S.L., Gong, S., Ramakrishnan, C., et al. (2011). Recombinase-driver rat lines: tools, techniques, and optogenetic application to dopamine-mediated reinforcement. Neuron *72*, 721–733.

Woo, D.H., Han, K.-S., Shim, J.W., Yoon, B.-E., Kim, E., Bae, J.Y., Oh, S.-J., Hwang, E.M., Marmorstein, A.D., Bae, Y.C., et al. (2012). TREK-1 and Best1 channels mediate fast and slow glutamate release in astrocytes upon GPCR activation. Cell *151*, 25–40.

Zhou, H., Falkenburger, B.H., Schulz, J.B., Tieu, K., Xu, Z., and Xia, X.G. (2007). Silencing of the Pink1 gene expression by conditional RNAi does not induce dopaminergic neuron death in mice. Int. J. Biol. Sci. *3*, 242–250.